LETTER

doi:10.1038/nature14429

Cell–intrinsic adaptation of lipid composition to local crowding drives social behaviour

Mathieu Frechin[1], Thomas Stoeger[1,2], Stephan Daetwyler[1], Charlotte Gehin[3], Nico Battich[1,2], Eva-Maria Damm[4], Lilli Stergiou[4], Howard Riezman[3] & Lucas Pelkmans[1]

Cells sense the context in which they grow to adapt their phenotype and allow multicellular patterning by mechanisms of autocrine and paracrine signalling[1,2]. However, patterns also form in cell populations exposed to the same signalling molecules and substratum, which often correlate with specific features of the population context of single cells, such as local cell crowding[3]. Here we reveal a cell-intrinsic molecular mechanism that allows multicellular patterning without requiring specific communication between cells. It acts by sensing the local crowding of a single cell through its ability to spread and activate focal adhesion kinase (FAK, also known as PTK2), resulting in adaptation of genes controlling membrane homeostasis. In cells experiencing low crowding, FAK suppresses transcription of the ABC transporter A1 (ABCA1) by inhibiting FOXO3 and TAL1. Agent-based computational modelling and experimental confirmation identified membrane-based signalling and feedback control as crucial for the emergence of population patterns of ABCA1 expression, which adapts membrane lipid composition to cell crowding and affects multiple signalling activities, including the suppression of ABCA1 expression itself. The simple design of this cell-intrinsic system and its broad impact on the signalling state of mammalian single cells suggests a fundamental role for a tunable membrane lipid composition in collective cell behaviour.

Adherent tissue culture cells spread out their cell surface more when experiencing low local crowding than high local crowding, resulting in a higher number of focal adhesions, sites of cellular attachment to the extracellular matrix (ECM), and higher levels of activated FAK (Extended Data Fig. 1a). FAK is recruited to focal adhesions, where it undergoes autophosphorylation, and subsequently recruits and phosphorylates phosphatidylinositol-3-OH kinase (PI(3)K) and many other proteins involved in signalling, cell adhesion and cytoskeletal dynamics[4–6]. FAK may thus, in a cell-intrinsic manner, sense local cell crowding by reacting to the available space and mechanical constraints imposed during cell population growth[7,8], and signal this to downstream cellular functions. To test this, we compared the extent of adaptation of the transcriptome to cellular crowding in adherent embryonic fibroblasts from a FAK-knockout mouse (FAK-KO) with cells from the same background in which FAK was stably re-expressed (FAK-rescue).

A total of 1,014 genes (~5% of the whole genome) adapt their transcript abundance to cellular crowding, of which 80% required the presence of FAK to adapt (Fig. 1a). Although FAK induces genes related to cell growth and proliferation (Extended Data Fig. 1b), it suppresses genes involved in membrane and organelle homeostasis (Fig. 1b) in cells experiencing low crowding, amongst which are 4 ATP-binding cassette (ABC) transporters (*Abca1*, *Abca6*, *Abca9* and *Abcg2*) (Extended Data Fig. 1c). *Abca1* was the overall second most strongly suppressed (~14-fold) gene by FAK (Fig. 1a) and the strongest hit amongst all genes in functional annotation terms related to membrane organization (Fig. 1b). ABC transporters mediate the transport of various substrates across membranes, including phospholipids and cholesterol[9,10].

Single-molecule fluorescence *in situ* hybridization and automated image analysis[3,11] confirmed the transcriptomics results at the single-cell level, showing that FAK controls the abundance of *Abca1* transcripts in single cells to local crowding (Fig. 1c and Extended Data Fig. 1d, e). This adaptation involves low (1–20) and highly variable transcript copy numbers (Extended Data Fig. 1d), and also occurs in the presence of growth factors and cytokines in the medium (Extended Data Fig. 1f).

Predicted candidate transcription factors (see Supplementary Information and Supplementary Table 2) were tested for their involvement in this adaptation using RNA-mediated interference (RNAi) in cells that lack FAK (FAK-KO) and thus highly express *Abca1* independent of crowding. RNAi of *Foxo3*, *Tal1* and *Stat4*, as well as *Lxrb* (liver X receptor beta, also known as *Nr1h2*), the canonical transcription factor driving expression of ABCA1 (ref. 12), reduced *Abca1* transcript abundance in these cells by ~50% (Extended Data Fig. 2a). As TAL1 and FOXO3 are phosphorylated by the serine/threonine kinase AKT, which is activated by PI(3)K downstream of FAK[5], leading to rapid degradation of TAL1 (ref. 13) and inactivation of FOXO3 (ref. 14), we focused on these transcription factors. Chromatin immunoprecipitation (ChIP) experiments (Extended Data Fig. 2b) revealed that in cells lacking FAK, both FOXO3 and TAL1 bind to *Abca1* chromatin independent of cellular crowding. In cells expressing FAK, FOXO3 and TAL1 bind to *Abca1* chromatin at closely located positions only when cells experience high crowding (Fig. 2a). This is in contrast to LXRB, which constitutively binds to *Abca1* chromatin independent of cellular crowding or the presence of FAK (Fig. 2a). Furthermore, western blots of multiple adherent cell lines revealed that cells experiencing low crowding contain higher levels of phosphorylated PI(3)K, AKT and FOXO3 and lower levels of TAL1 than cells experiencing high crowding. Consequently, these cells express a low amount of ABCA1 protein at low cellular crowding. Inhibition of PI(3)K (by wortmannin or LY-294002) lack of FAK (FAK-KO), or inhibition of FAK (by Y15) abolished these differences, leading to ABCA1 expression also in cells experiencing low crowding (Fig. 2b–e and Extended Data Fig. 2c–e). These effects were observed in mouse embryonic fibroblasts, human lung epithelial cells and freshly isolated human keratinocytes. Micropatterns confirmed that cell crowding-dependent expression of ABCA1 stems from the available space of a single cell to adhere to, consistent with a cell-intrinsic mechanism of adaptation (Extended Data Fig. 2f).

To understand if this cell-intrinsic mechanism can drive multicellular pattern formation, we applied single-cell mathematical modelling and computer simulation using a coupled two-level agent-based modelling[15] and differential equation approach (Supplementary Information (mathematical appendix)). The agent-based model simulates the dynamic behaviour of focal adhesions (Supplementary Video 1) and their adhesion potential in multiple single cells of a

[1]Faculty of Sciences, Institute of Molecular Life Sciences, University of Zurich, 8057 Zurich, Switzerland. [2]Life Science Zurich Graduate School, Ph.D. program in Systems Biology. ETH Zurich and University of Zurich, 8057 Zurich, Switzerland. [3]Department of Biochemistry, University of Geneva, 1205 Geneva, Switzerland. [4]Institute of Molecular Systems Biology, ETH Zurich, 8057, Zurich, Switzerland.

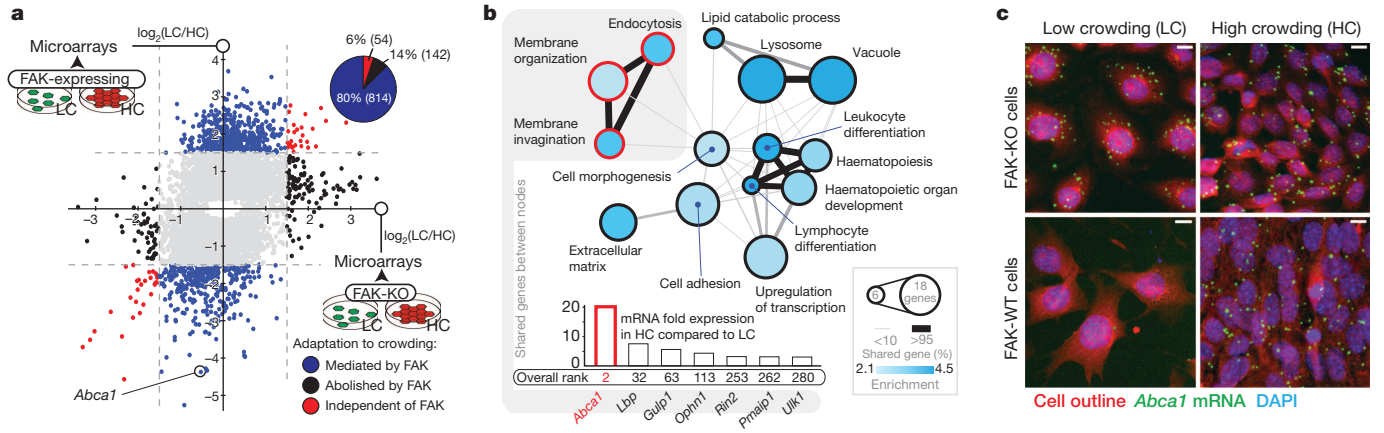

Figure 1 | Adaptation of the transcriptome to cellular crowding. **a**, Scatter plot of the $\log_2$ ratio of transcript abundance in cells experiencing high crowding (HC) over low crowding (LC) in mouse embryonic fibroblasts (MEFs) expressing (FAK-WT, *y* axis) or lacking FAK (FAK-KO, *x* axis). Significance threshold (straight lines): $|\log_2(LC/HC)| > 1.5$. **b**, Gene Ontology enrichment network of genes suppressed by FAK in cells experiencing low crowding. Node colour: enrichment, node size: number of genes, edge width: number of overlapping genes between nodes. **c**, Branched DNA (bDNA) single-molecule FISH against *Abca1* transcripts in FAK-KO (representative of 1.2×10^4 cells) or FAK-WT (representative of 1.5×10^4 cells) MEFs experiencing low or high crowding. DAPI, 4′,6-diamidino-2-phenylindole. Scale bars, 10 μm.

growing cell population (Fig. 3a, Supplementary Video 2 and Supplementary Information). Through indirect constraints that cells impose on each other, emergent properties at both the single-cell and the cell population level arise, including the formation of regions with higher and lower local cell crowding and the emergence of cell polarization and directed migration, agreeing with time-lapse measurements of populations of proliferating cells (Extended Data Fig. 3a–d). In the model, the adhesion potential of each simulated focal adhesion is then used to promote the activation of FAK through an autophosphorylation-based positive feedback loop (Extended Data Fig. 4a). This predicts the appearance of a stable pattern of activated FAK in a population of cells as observed in experiments (Fig. 3b, Supplementary Video 3 and Extended Data Fig. 5a–d).

When modelling suppression of *ABCA1* transcription downstream of activated FAK, we discovered that a gradual pattern of ABCA1 in a growing cell population only emerges when intracellular signal processing is coupled to the timescale at which changes in cellular crowding occur (Fig. 3b and Extended Data Figs 3e and 4b–d), adapted by a feedback mechanism (Fig. 3b, Extended Data Figs 3e and 6a and Supplementary Video 3). Timescale coupling could be achieved by the property of the membrane to act as a storage for phosphatidylinositol-3,4,5-triphosphate ($PtdIns(3,4,5)P_3$ or PIP_3) production by PI(3)K, while adaptation may be achieved by the ability of ABCA1 to alter physical properties of the membrane[16] leading to a decreased lipid ordering and increased diffusion rate of lipids[17], which affects the probability of AKT activation on the membrane by phosphoinositide-dependent kinase 1 (PDK1)[18,19]. We thus modelled the membrane as a 'tunable capacitor' (Fig. 3b and Extended Data Fig. 3e) that stores PIP_3 and that can be perturbed by ABCA1 in its capacity to activate AKT. This generates a pattern of ABCA1 expression similar to experimental observations that is insensitive to fluctuations in most parameters and primarily depends on the strength of ABCA1 feedback (Extended Data Fig. 6b–d). It also recapitulates the dynamics of ABCA1 down-regulation in scratch assays, when cells at high local crowding suddenly become exposed to free space (Extended Data Fig. 4f, g).

To investigate the existence of ABCA1 feedback on the capacitor function of the membrane, we examined whether the naturally observed crowding-dependent cell-to-cell variability in ABCA1

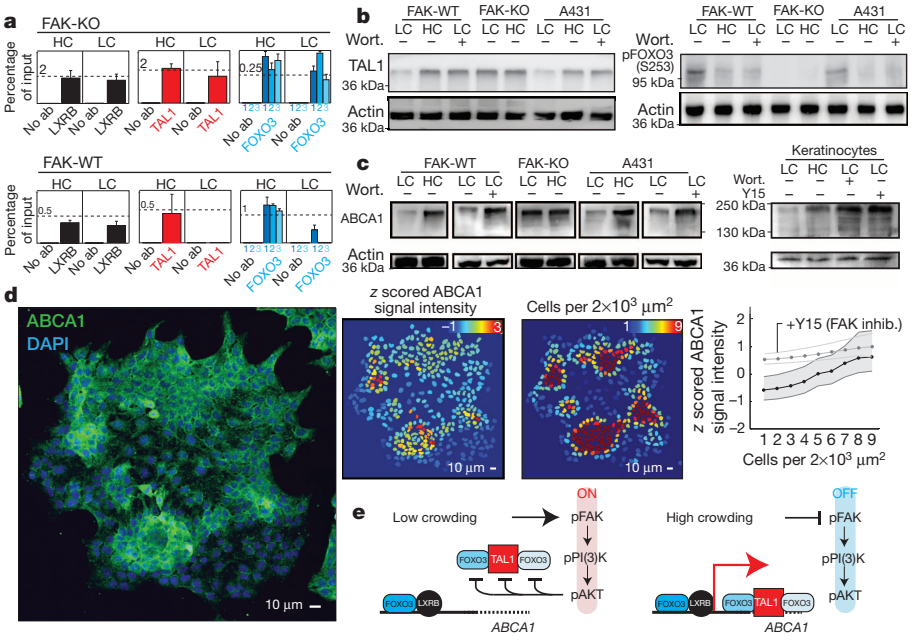

Figure 2 | FAK suppresses ABCA1 expression in cells at low crowding via TAL1 and FOXO3. **a**, ChIP of *Abca1* ($n = 3$ biological replicates, each mean of 3 technical replicates, s.d.) in FAK-KO and FAK-WT MEFs at low or high crowding. No ab, no antibody. **b**, Western blots of pFOXO3 and TAL1 levels in FAK-WT and FAK-KO MEFs, and A431 (human epidermoid carcinoma) cells at low crowding, high crowding, or low crowding + wortmannin. **c**, Western blots of ABCA1 levels as above, including in primary human keratinocytes and upon treatment with Y15 (FAK inhibitor). **d**, Immunofluorescence imaging of ABCA1 in a population of A431 cells (left, representative of 10^4 cells), quantified single-cell intensities of ABCA1 staining (centre) and local cell crowding (right). Curves, single-cell ABCA1 intensities against local cell crowding with or without Y15. Interquartile area in grey, n (single cells) $> 10^4$. **e**, Diagram of the FAK–ABCA1 pathway at low and high crowding. pFAK, phosphorylated FAK.

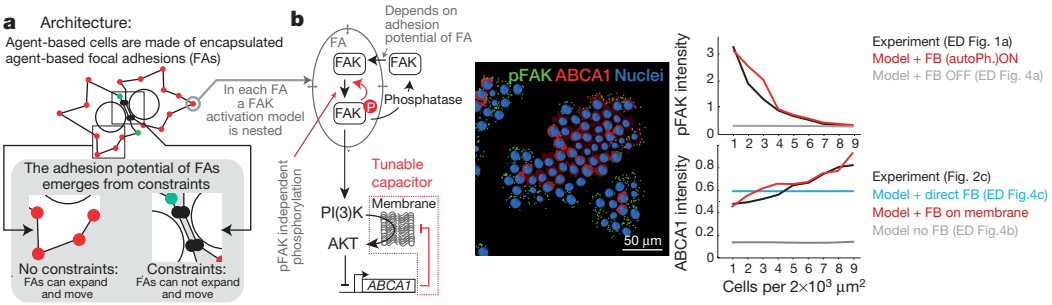

Figure 3 | Multi-scale model of the FAK–ABCA1 system. **a**, Architecture of agent-based modelled single cells encapsulating multiple agent-based modelled focal adhesions. **b**, Model of FAK activation nested in each focal adhesion, influenced by the adhesion potential of each focal adhesion emerging from **a** (left, top part). Model-simulated pFAK levels in single cells (centre image, green signal, representative of all simulations using the same parameters, this run: 10^3 cells) and quantification (right, top graph) against local cell crowding without (grey, Extended Data Fig. 4a) and with (red) positive feedback (FB), experiments in black (Extended Data Fig. 1a). Control of *ABCA1* transcription by FAK using a tunable membrane capacitor topology, which involves PI(3)K and AKT and feedback by ABCA1 (left, bottom part). Model-simulated ABCA1 levels in single cells (centre, red signal), and quantification (right, bottom graph) against local cell crowding without feedback (grey, Extended Data Fig. 4b), with direct feedback (light blue, Extended Data Fig. 4c), and with tunable capacitor (red). Experiments in black.

expression causes changes in membrane lipid composition. Cells experiencing high crowding have a strikingly different lipid composition than cells experiencing low crowding (Fig. 4a and Supplementary Table 3). Cells experiencing low crowding which expressed ABCA1 at levels naturally found in cells experiencing high crowding. (Extended Data Fig. 7a) have a lipid composition more closely resembling that of cells experiencing high crowding (Fig. 4a and Extended Data Fig. 7b). In particular, cells at low crowding have a higher amount of free cholesterol, higher levels of cholesteryl esters (Fig. 4b and Extended Data Fig. 7c), more lipid droplets (Extended Data Fig. 7f), a higher ratio of glucosylceramide over ceramide (GlcCer/Cer) (indicative of glycosphingolipid biosynthesis rate), higher levels of saturated lipids, and lower levels of monounsaturated and polyunsaturated lipids than cells at high crowding (Fig. 4b and Extended Data Fig. 7d, e). In cells experiencing high crowding, plasmid-driven expression of ABCA1 did not alter lipid composition (Fig. 4a, b, and Extended Data Fig. 7b–e). As a consequence, cells experiencing high crowding display lower membrane lipid ordering than cells experiencing low crowding (Fig. 4c), mediated by the crowding-dependent expression of ABCA1 (Extended Data Fig. 7g). Cells that lack FAK and thus express high levels of ABCA1 contain less cholesterol and less of the glycosphingolipid GM1 and display lower membrane lipid ordering than cells expressing FAK (Extended Data Fig. 7h, i).

Similarly, we found that ABCA1 levels influence the amount of S241-phosphorylated PDK1 and T308-phosphorylated AKT (Fig. 4d). Accordingly, levels of T308-phosphorylated AKT are higher in cells experiencing low crowding than cells experiencing high crowding (Fig. 4e). Pharmacological inhibition of ABCA1 abolished this pattern, increasing the level of T308-phosphorylated AKT in cells experiencing high crowding, as predicted by the model when the

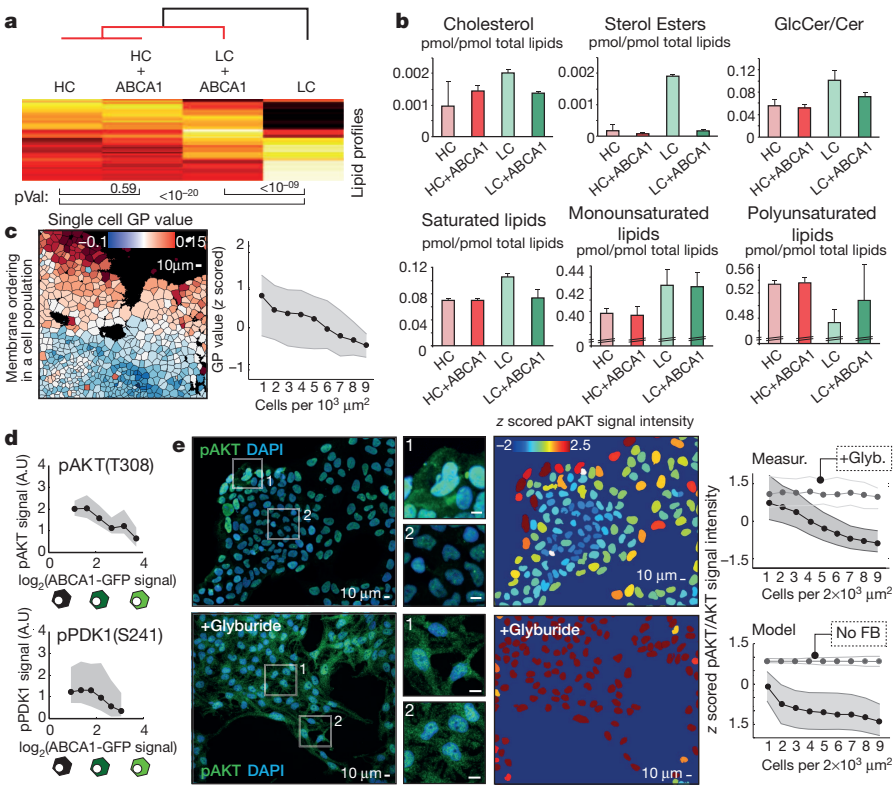

Figure 4 | The FAK–ABCA1 system adapts membrane lipid composition, ordering and signalling to local crowding. **a**, Hierarchical clustering of lipid profiles, see Extended Data Fig. 6b and Supplementary Table 3. *P* values determined by *t*-test. **b**, Histograms of selected lipid species (for free cholesterol in nmol per cell, see Extended Data Fig. 7c). For *P* values (*t*-test), see Extended Data Fig. 7d ($n = 4$ biological replicates, each the mean of 4 technical replicates, s.d.). **c**, *Z*-scored general polarization (GP) values (see Extended Data Fig. 7g) per single A431 cells (left) stained with Laurdan against local cell crowding (right) (interquartile area in grey, number of single cells $> 3 \times 10^3$). **d**, The effect of levels of ABCA1–GFP, randomly expressed from a plasmid in A431 cells at low crowding on pAKT and pPDK1 in single cells (interquartile area in grey). **e**, Untreated (top panels) or glyburide-treated (bottom panels) A431 cells immunostained against pAKT (T308). Nucleus segmentation images are colour-coded for pAKT levels. Top curves (left): single-cell pAKT levels against local crowding in absence (grey) or presence of glyburide (white) (n single cells $> 10^4$). Bottom curves: model-predicted pAKT levels against local crowding with (grey) or without (white) feedback (interquartile areas in grey).

double-negative feedback is removed (Fig. 4e). In addition, exogenous loading of the membrane with cholesterol and the glycosphingolipid GM1, as well as pharmacological inhibition of ABCA1, increases the level of phosphorylated PDK1 and AKT in cells lacking FAK (Extended Data Fig. 7j). Thus, ABCA1 inhibits the FAK-induced signalling pathway that suppresses its own transcription by adapting membrane lipid composition, confirming the membrane-based feedback predicted by the model as a requirement for gradual patterning. We made similar observations for levels of phosphorylated STAT3 and PAK1/2, which are respectively an effector of cytokine receptors and of the small GTPase RAC1, both sensitive to membrane lipid composition (Extended Data Fig. 8)[20,21]. This indicates that the adaptation of membrane lipid composition to local crowding by the FAK–ABCA1 system influences multiple signalling pathways in cells, including those involved in cell motility and paracrine signalling.

We have uncovered a cell-intrinsic molecular mechanism that allows patterning of membrane lipid composition and signalling according to local crowding in a cell population. Several genes with roles in membrane homeostasis may participate in this patterning system, including multiple ABC transporters and lipid-processing enzymes (see Supplementary Table 1, Extended Data Fig. 9 and Supplementary Discussion). In our minimal model, pattern formation of membrane lipid composition only requires variation in the extent of cellular crowding to emerge as cells proliferate. Patterning is subsequently promoted and stabilized by feedback loops without the need for specific cell–cell communication. Because lipid composition affects many membrane protein activities, adapting it to local crowding may have a fundamental role in controlling cellular behaviour within a social context, from colony formation in unicellular organisms[22] to collective cell migration[23], haematopoiesis[24] and T cell activation[25], and the control of epithelial cell proliferation in multicellular organisms[26].

Our work indicates a crucial role for membrane-based signalling in this cell-intrinsic system, in which the membrane may act as a capacitor that converts signals to the correct timescale and is tuned by enzymes that alter membrane lipid composition and ordering in a feedback mechanism. Both timescale adaptation and feedback are required for gradual patterns in a growing cell population to emerge. It will now be important to unravel how such a tunable capacitor operates mechanistically, and to generalize this concept to the possible uses of cellular structures in signal computation.

Online Content Methods, along with any additional Extended Data display items and Source Data, are available in the online version of the paper; references unique to these sections appear only in the online paper.

Received 25 September 2014; accepted 25 March 2015.
Published online 25 May 2015.

1. Kicheva, A., Cohen, M. & Briscoe, J. Developmental pattern formation: insights from physics and biology. *Science* **338,** 210–212 (2012).
2. Tabata, T. Genetics of morphogen gradients. *Nature Rev. Genet.* **2,** 620–630 (2001).
3. Snijder, B. *et al.* Population context determines cell-to-cell variability in endocytosis and virus infection. *Nature* **461,** 520–523 (2009).
4. Guan, J. L. & Shalloway, D. Regulation of focal adhesion-associated protein tyrosine kinase by both cellular adhesion and oncogenic transformation. *Nature* **358,** 690–692 (1992).
5. Schaller, M. D. Cellular functions of FAK kinases: insight into molecular mechanisms and novel functions. *J. Cell Sci.* **123,** 1007–1013 (2010).
6. Mitra, S. K., Hanson, D. A. & Schlaepfer, D. D. Focal adhesion kinase: in command and control of cell motility. *Nature Rev. Mol. Cell Biol.* **6,** 56–68 (2005).
7. Puliafito, A. *et al.* Collective and single cell behavior in epithelial contact inhibition. *Proc. Natl Acad. Sci. USA* **109,** 739–744 (2012).
8. Piccolo, S., Dupont, S. & Cordenonsi, M. The biology of YAP/TAZ: Hippo signaling and beyond. *Physiol. Rev.* **94,** 1287–1312 (2014).
9. Tarling, E. J., Vallim, T. Q. D. A., Edwards, P. & a.. Role of ABC transporters in lipid transport and human disease. *Trends Endocrinol. Metab.* **24,** 342–350 (2013).
10. Lawn, R., Wade, D. & Garvin, M. The Tangier disease gene product ABC1 controls the cellular apolipoprotein-mediated lipid removal pathway. *J. Clin. Invest.* **104,** 25–31 (1999).
11. Battich, N., Stoeger, T. & Pelkmans, L. Image-based transcriptomics in thousands of single human cells at single-molecule resolution. *Nature Methods* **10,** 1127–1133 (2013).
12. Costet, P., Luo, Y., Wang, N. & Tall, A. R. Sterol-dependent transactivation of the ABC1 promoter by the liver X receptor/retinoid X receptor. *J. Biol. Chem.* **275,** 28240–28245 (2000).
13. Palamarchuk, A. *et al.* Akt phosphorylates Tal1 oncoprotein and inhibits its repressor activity. *Cancer Res.* **65,** 4515–4519 (2005).
14. Brunet, A. *et al.* Akt promotes cell survival by phosphorylating and inhibiting a forkhead transcription factor. *Cell* **96,** 857–868 (1999).
15. Holcombe, M. *et al.* Modelling complex biological systems using an agent-based approach. *Integr. Biol. (Camb)* **4,** 53–64 (2012).
16. Zarubica, A. *et al.* Functional implications of the influence of ABCA1 on lipid microenvironment at the plasma membrane: a biophysical study. *FASEB J.* **23,** 1775–1785 (2009).
17. Saffman, P. G. & Delbrück, M. Brownian motion in biological membranes. *Proc. Natl Acad. Sci. USA* **72,** 3111–3113 (1975).
18. Lasserre, R. *et al.* Raft nanodomains contribute to Akt/PKB plasma membrane recruitment and activation. *Nature Chem. Biol.* **4,** 538–547 (2008).
19. Landry, Y. D. *et al.* ATP-binding cassette transporter A1 expression disrupts raft membrane microdomains through its ATPase-related functions. *J. Biol. Chem.* **281,** 36091–36101 (2006).
20. Shah, M., Patel, K., Fried, V. A. & Sehgal, P. B. Interactions of STAT3 with caveolin-1 and heat shock protein 90 in plasma membrane raft and cytosolic complexes: preservation of cytokine signaling during fever. *J. Biol. Chem.* **277,** 45662–45669 (2002).
21. del Pozo, M. A. *et al.* Integrins regulate Rac targeting by internalization of membrane domains. *Science* **303,** 839–842 (2004).
22. Vlamakis, H., Chai, Y., Beauregard, P., Losick, R. & Kolter, R. Sticking together: building a biofilm the *Bacillus subtilis* way. *Nature Rev. Microbiol.* **11,** 157–168 (2013).
23. Friedl, P. & Gilmour, D. Collective cell migration in morphogenesis, regeneration and cancer. *Nature Rev. Mol. Cell Biol.* **10,** 445–457 (2009).
24. Yvan-Charvet, L. *et al.* ATP-binding cassette transporters and HDL suppress hematopoietic stem cell proliferation. *Science* **328,** 1689–1693 (2010).
25. Bensinger, S. J. *et al.* LXR signaling couples sterol metabolism to proliferation in the acquired immune response. *Cell* **134,** 97–111 (2008).
26. Lee, B. H. *et al.* Dysregulation of cholesterol homeostasis in human prostate cancer through loss of ABCA1. *Cancer Res.* **73,** 1211–1218 (2013).

Supplementary Information is available in the online version of the paper.

Acknowledgements We thank B. Snijder for help with single-cell Laurdan quantification, P. Liberali for help with imaging of cell-to-cell variability, Y. Yakimovich for IT infrastructure support, and all members of the laboratory for discussions and support. M.F. was supported by an EMBO and a Marie Curie (301650) fellowship. E.-M.D. was supported by an Oncosuisse fellowship, L.S. was supported by a Bonizzi Theler fellowship. This work is supported by the University of Zurich and the SystemsX.ch RTD Project LipidX.

Author Contributions L.P. supervised and conceived the project, M.F., T.S., E.-M.D. and L.S. performed experiments, C.G. and H.R. performed lipid mass spectrometry, M.F. and N.B. developed computational image analysis methods, M.F. and L.P. performed data analysis, M.F. and S.D. developed mathematical models, M.F. performed mathematical modelling, L.P. and M.F. wrote the manuscript.

Author Information The microarray data set has been uploaded to the NCBI Gene Expression Omnibus as record GSE43873. Reprints and permissions information is available at www.nature.com/reprints. The authors declare no competing financial interests. Readers are welcome to comment on the online version of the paper. Correspondence and requests for materials should be addressed to L.P. (lucas.pelkmans@imls.uzh.ch).

METHODS

Cell culture. Media and reagents were from GibcoBRL. Wild-type MEFs (FAK-WT), or knockout for FAK (FAK-KO), and A431 cells were purchased from ATCC. Mouse embryonic fibroblasts rescued for FAK (FAK-rescue) were a gift from C. Hauck (University of Konstanz, Germany). E. Reichmann and L. Pontiggia provided keratinocyte primary cells (UZH, Zurich). Standard growth conditions were the following, cells were incubated 3 to 4 days using DMEM containing 10% FBS and 1× glutamine (+135 μg ml^{-1} hygromycinB for the FAK-rescue cells) at 37°C under 5% CO_2. Initial cell number was 2×10^5 to 2.5×10^5 cells for 10-cm dishes 3×10^4 to 5×10^4 cells per well for 12 wells plates containing 13 mm coverslips and 2×10^3 to 2.5×10^3 cells per well for 96-well plates. All our cell lines are tested on a monthly basis for mycoplasma contamination using chemiluminescent assay. The service is independent, centralized for all the UZH and provided at the institute of virology of the UZH. Once the desired population pattern is reached (see video in ref. 3, Snijder *et al.* 2009) cells are serum deprived for approximately 12 h and used for subsequent preparations. Wortmannin (100 nM), Y15 (25 μM), LY-294002 (10 μM) and glyburide (25 μM) treatments were performed over approximately 12 h before preparation. Coverslips were mounted on glass slide using Immu-Mount (Thermo Scientific), a water-based mounting medium.

Plasmid transfection. FAK-WT cells grown in 96-well plates or 10-cm dishes were transfected respectively with 80 ng per well or 4 μg of ABCA1 construct carried in the pEGFP-N1 backbone mixed with 0.2 or 10 μl lipofectamine2000 following the manufacturer's specifications. Homo sapiens *ABCA1* coding sequence was synthesized *de novo* and inserted between SacI and SacII restriction sites. The cloned *ABCA1* sequence corresponds to the full-length consensus coding sequence CCDS6762.1.

Cholesterol and GM1 staining. Cells were quickly washed with successive 1× PBS, 5% delipidated BSA, 1× PBS and fixed for 4 min with 4% PFA. Cholesterol was stained using 0.01 mg ml^{-1} filipin (Sigma) for 20 min, after two washes of 5 min in PBS, surface GM1 was stained using 0.2 μg ml^{-1} cholera toxin subunit B (Alexa Fluor 555 conjugate, Invitrogen) for 10 min.

Laurdan live staining. Cells were grown in ibidi μ-Slide 8 well chambers under standard conditions. Five minutes before acquisition, cells were mounted on the microscope (see microscope section) with environmental control and live stained by addition of 6-dodecanoyl-2-dimethylaminonaphthalene (Laurdan, Molecular Probes) and Draq5 (Cell Signaling) at 5 and 0.5 μM final concentrations directly in the medium. Images were acquired within the next 2 min.

Immunostaining. Unless specified, cells were grown following standard procedures. Fixation was performed with 4%PFA for 10 min, permeabilization with 0.1% Triton X-100 for 10 min, blocking with 1% BSA, 50 mM NH_4Cl for 30 min. Primary and secondary antibodies were diluted in blocking solution, treatments were separated by two 30-min PBS washes. Secondary antibody was applied for 1 h (Alexa Fluor 488 or 568 goat anti rabbit antibody, Invitrogen, 1 μg ml^{-1}). Nuclear staining is performed with 1 μM DAPI for 10 min and cell outlines are visualized with Alexa Fluor 647 carboxylic acid succinimidyl ester (Life Science, 10^{-4} dilution) staining for 10 min. For the pFAK staining, primary antibody was applied for 3 h (rabbit anti-pFAK (Y397) antibody, Cell Signaling no. 3283, 1:200) as well as for ABCA1 (rabbit anti-ABCA1 antibody, Abcam ab7360, 1:500). For pAKT (rabbit anti-pAKT (T308) antibody, Cell Signaling no. 2965, 1:1,000), pPDK1 (rabbit anti-pPDK1 (S241), no. 3061, Cell Signaling, 1:1,000), pSTAT3 (rabbit anti-pSTAT3 (T705) antibody, Cell Signaling no. 9131, 1:500) and pPAK1 (rabbit anti-pPAK1/2 (T423/T402) antibody, Cell Signaling no. 2601, 1:200) staining, primary antibody was applied overnight at 4°C.

mRNA bDNA-FISH experiments. FAK-WT cells were grown following standard conditions in 96-well plates. *Abca1* mRNA bDNA-FISH experiments and image based analysis were performed using the protocol and computational method published by our laboratory[11]. Briefly, cells were fixed, permeabilized, and protease K treated for the *Abca1* mRNA specific probe set to access properly its target sequences. A three-step treatment with successive pre-amplifier, amplifier and fluorescent probes hybridization allows the amplification of the mRNA probe signal and the visualization of single *Abca1* mRNAs. Nuclear staining was performed with 1 μM DAPI for 10 min. Cell outlines were visualized with Alexa Fluor 647 carboxylic acid succinimidyl ester (Life Science) (10^{-4} dilution) staining for 10 min.

Microscopes. Laurdan, filipin and cholera toxin B images were acquired with 40× magnification on a Leica SP5 confocal microscope equipped with a UV laser (λ, 355 nm) in addition to the usual set of visible light lasers, for proper stimulation of Laurdan and filipin. Confocal images of pFAK were acquired on a Zeiss LSM710 microscope with 40× magnification (Zeiss NA1.2, C-apochromat, Korr UV-VIS-IR), GFP-FAK total internal reflection fluorescence (TIRF) video images were acquired on a Nikon visiView microscope with 100× magnification. Immunostainings of ABCA1, pS6, pAKT, pPI(3)K, pSTAT3, pPAK1 and mRNA bDNA-FISH images were acquired on an automated Yokogawa CV7000 spinning disk microscope.

Image analysis. All image analysis was performed using CellProfiler[27] following the same procedure we used in previous publications[3,11,28], with the help of additional MATLAB scripts published previously for the calculation of cellular crowding[3] or written specifically for this study for Laurdan image analysis (see specific section). The general image analysis pipeline was as follows. First, nuclei were detected and segmented based on the DAPI or Draq5 stain using IdentifyPrimaryObjects CellProfiler module. Then, cell boundaries were estimated using nuclear propagation in IdentifySecondaryObjects CellProfiler module. Standard CellProfiler texture, intensity, size and shape features were extracted from nucleus and cell regions. We additionally implemented several image analysis steps for the purpose of detection of out of focus images and for the Support Vector Machine (SVM)-based classification[29] of poorly segmented nuclei.

Membrane ordering analysis. A dedicated CellProfiler module has been developed for this study (the code is available upon request) for defining automatically single-cell generalized polarization (scGP) values after nuclear and cell segmentation. This measurement is based on a previous publication[30] and works as follows: images of cells stained with Laurdan (see specific section above for details) are simultaneously acquired in the 400–460 nm (*I*1) and 470–530 nm (*I*2) wavelength windows after stimulation at 355 nm. The GP value is defined for each pixel following the formula:

$$\mathrm{pxGP} = \frac{I1 - I2}{I1 + I2}$$

The mean GP value of each single cell (scGP value) is then defined by the mean of all pxGP values contained in each segmented cell.

Microarray analysis. High and low crowding FAK-rescue and FAK-KO cells were grown for 24 h in 10-cm dishes, in 10 ml of standard medium (described in the cell culture and preparation section). High crowding cells were seeded at a concentration of 10^6 cells per ml and low crowding cells at 0.4×10^5 cells per ml. RNA preparations were done with the Qiagen RNeasy Mini Kit according to the manufacturer's manual, including the optional column DNase treatment.

The quality of the isolated RNA was determined with a NanoDrop ND 1000 (NanoDrop Technologies, Delaware, USA) and a Bioanalyzer 2100 (Agilent, Waldbronn, Germany). Only the samples with a 260/280 nm ratio between 1.8 and 2.1 and an RNA integrity number (RIN) higher than 8 were further processed. Total RNA samples (100 ng) were reverse-transcribed into double-stranded cDNA in presence of RNA poly-A controls, RNA Spike-In Kit, One-Colour (Agilent product number 5188-5282). The double-stranded cDNAs were *in vitro* transcribed in presence of Cy3-labelled nucleotides using a Low Input Quick Amp Labelling Kit, one-colour (Agilent product number 5190–2305). The Cy3-cDNA was purified using an ARNeasy mini kit, Qiagen (product number 74104 or 74106) and its quality and quantity was determined using NanoDrop ND 1000 and Bioanalyzer 2100. Only cDNA samples with a total cDNA yield higher than 2 μg and a dye incorporation rate between 8 pmol μg^{-1} and 20 pmo μg^{-1} were considered for hybridization.

Cy3-labelled cRNA samples (1.65 μg) were mixed with a Agilent Blocking Solution, subsequently randomly fragmented to 100–200 bp at 65°C with Fragmentation Buffer, and resuspended in Hybridization Buffer using a Gene Expression Hybridization Kit (Agilent product number 5188–5242). Target cRNA Samples (100 μl) were hybridized to Whole Mouse Genome 4×44k OligoMicroarrays (Agilent G4122F) for 17 h at 65°C. Arrays were then washed using Agilent GE Wash Buffers 1 and 2 (Agilent product number 5188–5326), according to the manufacturer's instructions (One-Colour Microarray-Based Gene Expression Analysis Manual, http://www.agilent.com). An Agilent Microarray Scanner (Agilent product number G2565BA) was used to measure the fluorescent intensity emitted by the labelled target. The microarray data set has been uploaded to the NCBI Gene Expression Omnibus as record GSE43873, reorganized and filtered data can be downloaded in the Supplementary Information section (MicroarrayData.xls).

Functional enrichment analysis. The Gene Ontology term enrichment analysis was done with DAVID[31,32] on genes significantly more expressed (absolute $\log_2$(low/high crowding) gene expression value over 1.5) in FAK-expressing cells. Functional groups shown in the two networks have an enrichment value superior than 2 and are composed of at least 5 genes.

Selection of candidate transcription factors. The 19 transcription factors screened in the FAK-KO cells for their potential effect on *Abca1* mRNA expression were selected using a combination of three approaches. (1) Candidates have a binding site in all of the top 10 FAK suppressed genes defined with the microarray data. To perform this comparison, we used the Pscan algorithm (http://www.beaconlab.it/pscan) with the JASPAR database[33] (http://jaspar.genereg.net/). (2) Transcription factors having the strongest GO enrichment for lipid

homeostasis or (3) having a reported ChIP binding site or an effect on expression for ABCA1 in the literature (Supplementary Table 2).

siRNA experiments. All siRNAs were purchased from Qiagen. FAK-KO cells were cultured in 24-well plates, using standard conditions until reaching approximately 60% confluency (48–60 h) and transfected by forward transfection. Per well, 25 pmol samples of siRNA were mixed in 25 µl of Opti-MEM and 0.5 µl of Lipofectamine RNAiMAX were mixed with 24.5 µl of Opti-MEM. After 5 min of incubation, solutions were mixed together and incubated for another 20 min at room temperature and transferred on the cultured cells for 60 h before RNA preparation.

qPCR screening. Silenced FAK-KO cells were washed with 1× PBS, RNA samples were prepared using NucleoSpinRNAII kit (Macherey Nagel), cDNA synthesis was carried out with the Transcriptor High Fidelity cDNA Synthesis Kit (Roche) using poly-dT primers, in both cases following the manufacturer's protocol. Quantitative real-time PCR was performed in 384-well plates in an AB7900HT qPCR device (Applied Biosystems) using the following primers, forward ABCA1: 5′-CTGTAGACCTGGAGAGAAGCTTTC-3′, reverse ABCA1: 5′-CAGCTCCA TGGACTTGTTGATGAG-3′ allowing amplification over the twelfth and thirteenth exons contained in all *ABCA1* mRNA variants, and forward GAPDH: 5′-TCAAGGCTGAGAACGGGAAGCTTG-3′, reverse GAPDH: 5′-AGCCTTCT CCATGGTGGTGAAGAC-3′. Relative mRNA amounts were calculated using GAPDH as an internal reference.

Western blotting. A431, FAK-WT and FAK-KO cells were cultured using standard conditions in 10-cm dishes. Low crowding cells were stopped after 2 to 2.5 days of growth, whereas high crowding cells were grown for 6 days (both including a final 12 h of serum starvation). Cells were washed with 1 × PBS and disrupted in lysis buffer (0.5% sodium deoxycholate, 150 mM NaCl, 50 mM Tris-HCl, pH 7.2, 0.1% SDS, 1% Triton X-100, 0.2% NaN_3), and 15 µg of each protein extract was separated using 10% PAGE except for ABCA1 western blotting where 50 µg of protein and 8% PAGE were used. Separated proteins were then transferred onto a membrane (Immobilon-P, 0.45 µm, Millipore) using the humid chamber method. Transfer conditions are 80 mA overnight for ABCA1 western blotting, 250 mA for 90 min otherwise. Membranes were blocked with 4% BSA proteins in 1× TBS-T (1× TBS, 0.1% Tween) for 1 h. Primary antibodies rabbit anti-pFAK (Cell Signaling no. 3283), rabbit anti-pPI(3)K (rabbit anti-pPI(3)K p85/p55 (T458/T199) antibody, Cell Signaling no. 4228), rabbit anti-pAKT ((T308) Cell Signaling no. 2965) were diluted at 1:1,000 and rabbit anti-actin (Cell Signaling no. 8456) at 1:5,000. Rabbit anti-TAL1 (Sc-12984, Santa Cruz) and rabbit anti-pFOXO3 (S253, no. 9466, Cell Signaling) were diluted at 1:200 and rabbit anti-ABCA1 (Abcam ab7360) at 1:500 in blocking buffer. HRP-conjugated secondary anti-mouse (no. 170-6516, BioRad) and anti-rabbit (no. 170-6515, BioRad) antibodies were diluted at 1:5,000 in the same buffer. Primary and secondary antibodies were applied overnight at 4°C and 60 min at room temperature, respectively. Signal was revealed with HRP substrate solution and imaged with a CCD camera (for antibody references see immunostaining section).

ChIP experiments. FAK-KO and FAK-WT cells were cultured using standard conditions in 10-cm dishes. Low crowding cells were stopped after 2 to 2.5 days of growth, whereas high crowding cells were grown for 6 days (both including a final 12 h of serum starvation). Experiments were carried out using the Chromatin Immunoprecipitation (ChIP) Assay Kit from Millipore following manufacturer's specifications except for the following changes. Fixation of cells was performed with 1.6 mM Di-thio bis-succinimidyl propionate (DSP) for 20 min, two short washes with 1× PBS at room temperature, and finally 1% paraformaldehyde for 20 min. 20 µg of anti-TAL1 (Sc-12984, Santa Cruz), anti-FOXO3 (07–702, Millipore) and anti-LXR beta (Sc-34341, Santa Cruz) primary antibodies was added for 15 h at 4°C to the pre-cleared supernatant. Protein A beads were then added for 4 h. Reversion of crosslinking was done for 12 h at 55°C.

Lipid mass spectrometry

Chemicals and lipid standards. DLPC 12:0/12:0 (850335), PE 17:0/14:1 (PE31:1, LM-1104), PI 17:0/14:1 (PI31:1, LM-1504), PS 17:0/14:1 (PS31:1, LM-1304), C17:0 ceramide (860517), C12:0 SM (860583) and Glucosyl C8:0 Cer (860540) were used as internal lipid standards and were purchased from Avanti Polar Lipids Inc. (Alabaster, AL). Ergosterol was used as sterol standard and was purchased from Fluka (Buchs, Switzerland). Methyl tert-butyl ether (MTBE) was from Fluka (Buchs). Methyl amine (33% in absolute ethanol) was from Sigma Aldrich (Steinheim, Germany). HPLC-grade chloroform was purchased from Acros (Geel, Belgium), liquid chromatography–mass spectrometry (LC–MS) grade methanol and LC–MS grade ammonium acetate were from Fluka. LC–MS grade water was purchased from Biosolve.

Cell culture. FAK-WT cells were cultured using standard conditions in 10-cm dishes. Low crowding cells were stopped after 2.5–3 days of growth while high crowding cells were grown for 6 days (both including a final 12 h of serum starvation). Cells were transfected with a human ABCA1-containing plasmid as described above or subjected to the transfection procedure without plasmid after one day of culture for low crowding cells or four days of culture for high crowding cells. Cells facing low or high crowding were collected two days after transfection. Cells were shortly washed with successively 1× PBS, 5% delipidated BSA, and three times with cold 1× PBS, scraped and pelleted at 800*g* for 5 min before lipid extraction.

Lipid analysis. Lipid extracts of 4 biological replicates of each of the 4 conditions (high crowding; high crowding +ABCA1; low crowding; low crowding +ABCA1) were prepared using the MTBE protocol[34] and measurements were made in 4 technical replicates, amounting to a total of 64 measurements at each mass spectrometer. Cell pellets were resuspended into 100 µl of water and transferred into a 2 ml Eppendorf tube. Then 360 µl methanol and a mix of internal standards were added (400 pmol DLPC, 1,000 pmol PE31:1, 1,000 pmol PI31:1, 3,300 pmol PS31:1, 2,500 pmol C12SM, 500 pmol C17Cer and 100 pmol C8GC). Samples were vortexed and 1.2 ml of MTBE was added. Samples were placed for 10 min on a multitube vortexer at 4°C (Lab-tek International) followed by an incubation for 1 h at room temperature on a shaker. Phase separation was induced by addition of 200 µl MS-grade water. After 10 min of incubation at room temperature, samples were centrifuged at 1,000*g* for 10 min. The upper (organic) phase was transferred into a 13 mm glass tube with a Teflon-lined cap and the lower phase was re-extracted with 400 µl artificial upper phase (MTBE/methanol/H_2O 10:3:1.5). In total, 1,500 µl of organic phase was recovered from each samples, split into three parts and dried in a CentriVap Vacuum Concentrator (Labconco). One part was treated by alkaline hydrolysis to enrich for sphingolipids and the other two aliquots were used for glycerophospholipid/phosphorus assay and sterol analysis, respectively. Glycerophospholipids were deacylated according to the method by Clarke & Dawson[35]. Briefly, 1 ml freshly prepared monomethylamine reagent (methylamine/H_2O/n-butanol/methanol at 5:3:1:4 (vol/vol)) was added to the dried lipid extract and then incubated at 53°C for 1 h in a water bath. Lipids were cooled to room temperature and then dried. For desalting, the dried lipid extract was resuspended in 300 µl water-saturated n-butanol and then extracted with 150 µl H_2O. The organic phase was collected, and the aqueous phase was reextracted twice with 300 µl water-saturated n-butanol. The organic phases were pooled and dried in a CentriVap Vacuum Concentrator.

Sterols analysis by gas chromatography–mass spectrometry (GC–MS). One-third of total lipid extract was resuspended in 500 µl of MS-grade chloroform/methanol (1:1) solution and injected into a VARIAN CP-3800 gas chromatogram equipped with a Factor Four Capillary Column VF-5ms 15 mm × 0.32 mm i.d. DF = 100. Identification and quantification of sterol species were performed using a VARIAN 320MS as described in ref. 36.

Phospholipids and sphingolipids analysis by electrospray ionization mass spectrometry (ESI-MS). Identification and quantification of phospholipid and sphingolipid molecular species were performed using multiple reaction monitoring with a TSQ Vantage Triple Stage Quadrupole Mass Spectrometer (Thermo Scientific) equipped with a robotic nanoflow ion source, Nanomate HD (Advion Biosciences). Each individual ion dissociation pathway was optimized with regard to collision energy. Lipid concentrations were calculated relative to the relevant internal standards as described in ref. 37 and then normalized to the total phosphorus content of each total lipid extract to adjust for difference in cell size, membrane content, and extraction efficiency.

Determination of total phosphorus content. The dried total lipid extract was resuspended in 250 µl chloroform/methanol (1:1) and 50 µl were placed into a 13 mm disposable pyrex tube. The solvent was completely evaporated and 0, 2, 5, 10, 20 µl of a 3 mM KH_2PO_4 standard solution were placed into separate pyrex tubes. To each tube 20 µl of water and 140 µl of 70% perchloric acid were added. Samples were heated at 180°C for 1 h in a hood. Tubes were then removed from the block and kept at room temperature for 5 min. Then 800 µl of freshly prepared H_2O/1.25% NH_4Molybdate (100 mg/8 ml H_2O)/10% ascorbic acid (100 mg/6 ml H_2O) in the ratio of 5:2:1 were added. Tubes were heated at 100°C for 5 min with a marble on each tube to prevent evaporation. Tubes were cooled at room temperature for 5 min. 100 µl of each sample was then transferred into a 96-well microplate and the absorbance at 820 nm was measured[38].

27. Carpenter, A. E. *et al.* CellProfiler: image analysis software for identifying and quantifying cell phenotypes. *Genome Biol.* **7,** R100 (2006).
28. Wippich, F. *et al.* Dual specificity kinase DYRK3 couples stress granule condensation/dissolution to mTORC1 signaling. *Cell* **152,** 791–805 (2013).
29. Rämö, P., Sacher, R., Snijder, B., Begemann, B. & Pelkmans, L. CellClassifier: supervised learning of cellular phenotypes. *Bioinformatics* **25,** 3028–3030 (2009).
30. Gaus, K., Zech, T. & Harder, T. Visualizing membrane microdomains by Laurdan 2-photon microscopy. *Mol. Membr. Biol.* **23,** 41–48 (2006).

31. Huang, D. W., Sherman, B. T. & Lempicki, R. A. Systematic and integrative analysis of large gene lists using DAVID bioinformatics resources. *Nature Protocols* **4,** 44–57 (2009).
32. Huang, d. W., Sherman, B. T., Lempicki, R. & a.. Bioinformatics enrichment tools: paths toward the comprehensive functional analysis of large gene lists. *Nucleic Acids Res.* **37,** 1–13 (2009).
33. Sandelin, A., Alkema, W., Engström, P., Wasserman, W. W. & Lenhard, B. JASPAR: an open-access database for eukaryotic transcription factor binding profiles. *Nucleic Acids Res.* **32,** D91–D94 (2004).
34. Matyash, V., Liebisch, G., Kurzchalia, T. V., Shevchenko, A. & Schwudke, D. Lipid extraction by methyl-tert-butyl ether for high-throughput lipidomics. *J. Lipid Res.* **49,** 1137–1146 (2008).
35. Clarke, N. G. & Dawson, R. M. *Alkaline O→N-transacylation.* 195**,** 301–306 (1981). A new method for the quantitative deacylation of phospholipids. *Biochem. J.* **195,** 301–306 (1981).
36. Guan, X. L., Riezman, I., Wenk, M. R. & Riezman, H. Yeast lipid analysis and quantification by mass spectrometry. *Methods Enzymol.* **470,** 369–391 (2010).
37. Epstein, S. *et al.* Activation of the unfolded protein response pathway causes ceramide accumulation in yeast and INS-1E insulinoma cells. *J. Lipid Res.* **53,** 412–420 (2012).
38. Rouser, G., Fleischer, S. & Yamamoto, A. Two dimensional thin layer chromatographic separation of polar lipids and determination of phospholipids by phosphorus analysis of spots. *Lipids* **5,** 494–496 (1970).

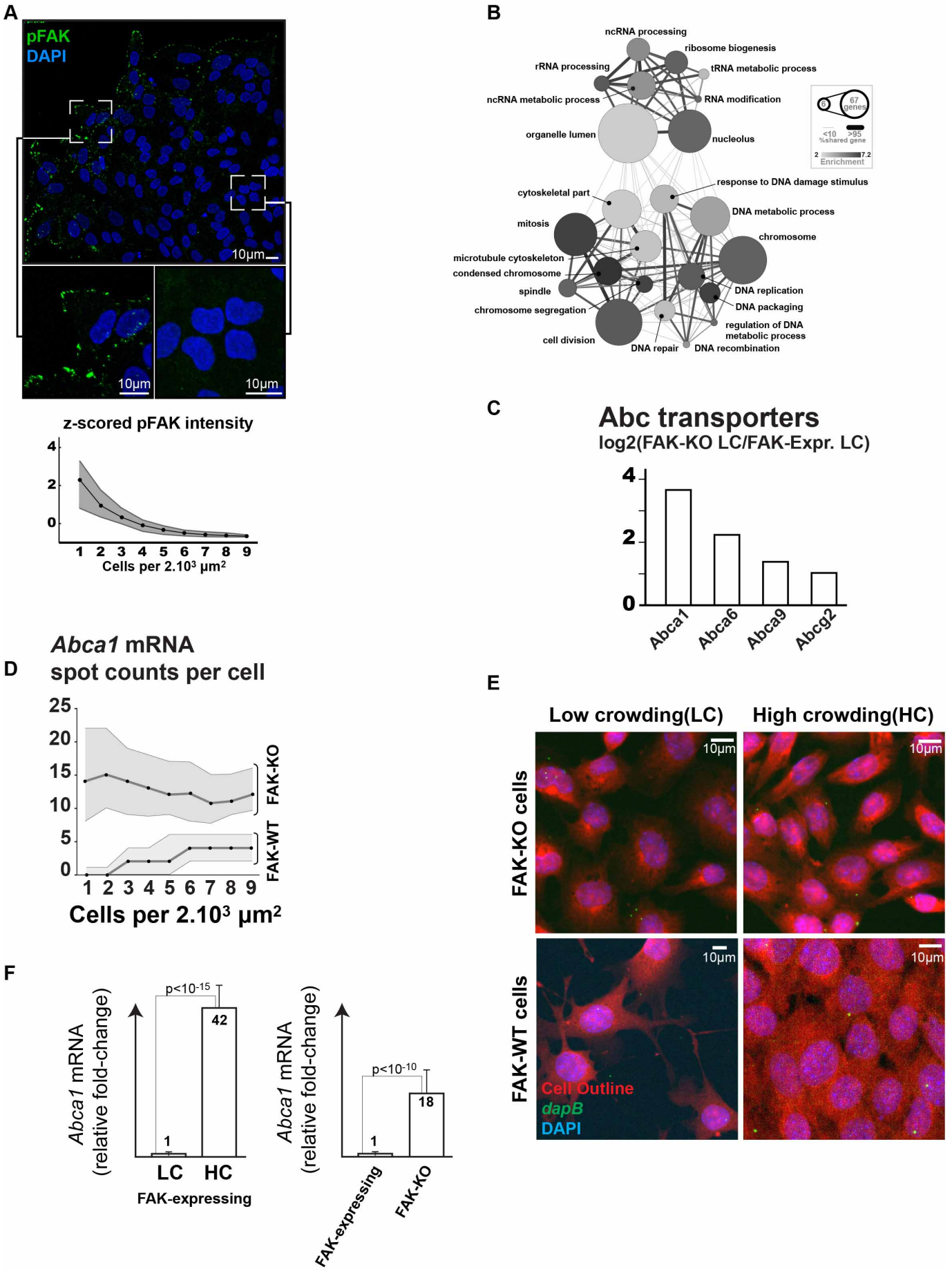

Extended Data Figure 1 | Adaptation of the transcriptome to cellular crowding. Related to Fig. 1. **a**, Immunofluorescence against phosphorylated FAK (Y397) in a population of A431 cells, corresponding curve shows single-cell phosphorylated FAK signals against local cell crowding (interquartile area is shown in grey, number of cells $>10^4$). **b**, Gene Ontology enrichment network of genes that are induced by FAK in cells experiencing low crowding. Greyscale indicates enrichment, node-size number of genes, edge width between nodes number of overlapping genes. **c**, Histogram of ABC transporters more expressed in cells lacking FAK compared to cells expressing FAK when facing low crowding. **d**, Single-cell transcript counts of *Abca1* in 1.2×10^4 FAK-KO and 1.5×10^4 FAK-WT cells experiencing increasing levels of local crowding (interquartile area in grey). **e**, Control experiment of bDNA single-molecule FISH against bacterial *dapB* transcripts in FAK-KO or FAK-WT cells experiencing low crowding or high crowding. Representative of 10^4 cells. **f**, Real-time PCR measurements of *Abca1* transcripts in cells at low and high local crowding in both FAK-expressing and FAK-KO cells in the presence of 10% FCS. Clearly, *Abca1* mRNA levels are much higher in FAK-expressing cells facing high crowding than in the same cells facing low crowding (s.d., $n = 4$ biological replicates each made of 3 technical replicates, $P < 10^{-15}$, *t*-test) but also in FAK-KO cells compared FAK-expressing cells (s.d., $n = 4$ biological replicates each made of 3 technical replicates, $P < 10^{-10}$, *t*-test). This indicates that FAK-dependent adaptation of *Abca1* transcription to cell crowding also operates in the presence of an abundant and homogeneous amount of growth factors and cytokines in the medium.

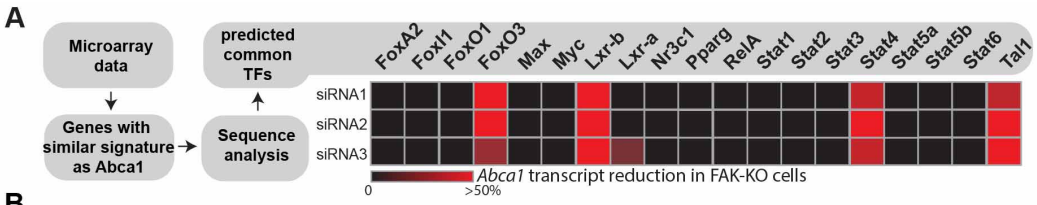

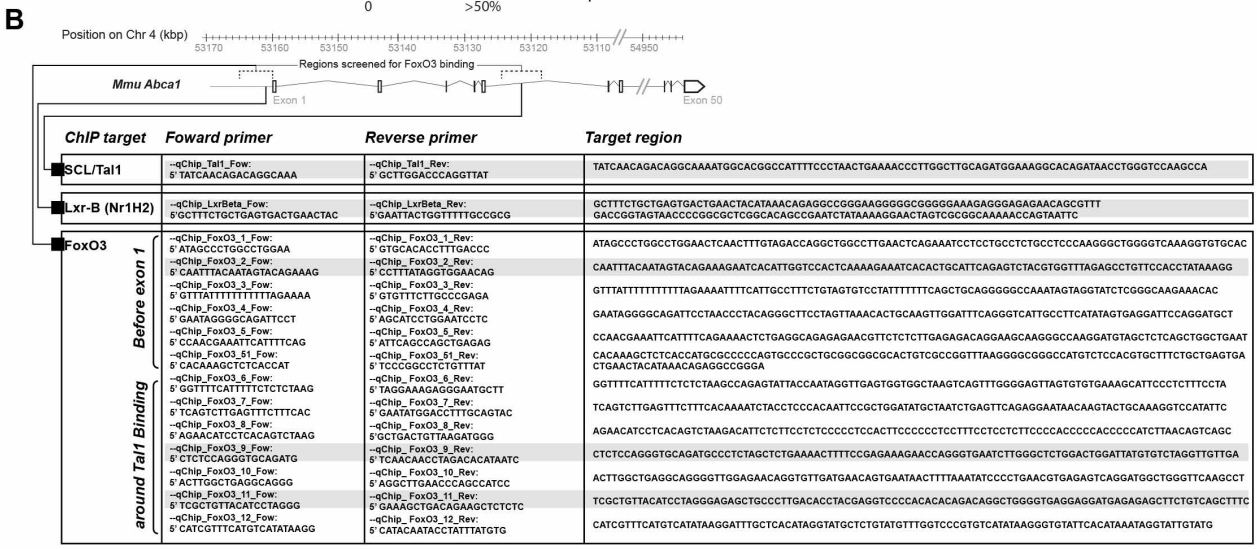

ChIP target	Foward primer	Reverse primer	Target region
SCL/Tal1	--qChip_Tal1_Fow: 5' TATCAACAGACAGGCAAAA	--qChip_Tal1_Rev: 5' GCTTGGACCCAGGTTAT	TATCAACAGACAGGCAAAATGGCACGGCCATTTTCCCTAACTGAAAACCCTTGGCTTGCAGATGGAAAGGCACAGATAACCTGGGTCCAAGCCA
Lxr-B (Nr1H2)	--qChip_LxrBeta_Fow: 5'GCTTTCTGCTGAGTGACTGAACTAC	--qChip_LxrBeta_Rev: 5'GAATTACTGGTTTTTGCCGCG	GCTTTCTGCTGAGTGACTGAACTACATAAACAGAGGCCGGGAAGGGGGCGGGGGAAAGAGGGAGAGAACAGCGTTT GACCGGTAGTAACCCCGGCGCTCGGCACAGCCGAATCTATAAAAGGAACTAGTCGCGGCAAAAACCAGTAATTC
FoxO3 — Before exon 1	--qChip_FoxO3_1_Fow: 5' ATAGCCCTGGCCTGGAA	--qChip_ FoxO3_1_Rev: 5' GTGCACACCTTTGACCC	ATAGCCCTGGCCTGGAACTCAACTTTGTAGACCAGGCTGGCCTTGAACTCAGAAATCCTCCTGCCTCTGCCTCCCAAGGGCTGGGGTCAAAGGTGTGCAC
	--qChip_FoxO3_2_Fow: 5' CAATTTACAATAGTACAGAAAG	--qChip_FoxO3_2_Rev: 5' CCTTTATAGGTGGAACAG	CAATTTACAATAGTACAGAAAGAATCACATTGGTCCACTCAAAAGAAATCACACTGCATTCAGAGTCTACGTGGTTTAGAGCCTGTTCCACCTATAAAGG
	--qChip_FoxO3_3_Fow: 5' GTTTATTTTTTTTTTTAGAAAA	--qChip_ FoxO3_3_Rev: 5' GTGTTTCTTGCCCGAGA	GTTTATTTTTTTTTTTAGAAAATTTTCATTGCCTTTCTGTAGTGTCCTATTTTTTTCAGCTGCAGGGGGCCAAATAGTAGGTATCTCGGGCAAGAAACAC
	--qChip_FoxO3_4_Fow: 5' GAATAGGGGCAGATTCCT	--qChip_ FoxO3_4_Rev: 5' AGCATCCTGGAATCCTC	GAATAGGGGCAGATTCCTAACCCTACAGGGCTTCCTAGTTAAACACTGCAAGTTGGATTTCAGGGTCATTGCCTTCATATAGTGAGGATTCCAGGATGCT
	--qChip_FoxO3_5_Fow: 5' CCAACGAAATTCATTTTCAG	--qChip_ FoxO3_5_Rev: 5' ATTCAGCCAGCTGAGAG	CCAACGAAATTCATTTTCAGAAAACTCTGAGGCAGAGAGAACGTTCTCTCTTGAGAGACAGGAAGCAAGGGCCAAGGATGTAGCTCTCAGCTGGCTGAAT
	--qChip_FoxO3_51_Fow: 5' CACAAAGCTCTCACCAT	--qChip_ FoxO3_51_Rev: 5' TCCCGGCCTCTGTTTAT	CACAAAGCTCTCACCATGCGCCCCCAGTGCCCGCTGCGGCGGCGCACTGTCGCCGGTTTAAGGGGCGGGCCATGTCTCCACGTGCTTTCTGCTGAGTGA CTGAACTACATAAACAGAGGCCGGGA
	--qChip_FoxO3_6_Fow: 5' GGTTTTCATTTTTCTCTCTAAG	--qChip_ FoxO3_6_Rev: 5' TAGGAAAGAGGCGAATGCTT	GGTTTTCATTTTTCTCTCTAAGCCAGAGTATTACCAATAGGTTGAGTGGTGGCTAAGTCAGTTTGGGGAGTTAGTGTGTGAAAGCATTCCCTCTTTCCTA
	--qChip_FoxO3_7_Fow: 5' TCAGTCTTGAGTTTCTTTCAC	--qChip_ FoxO3_7_Rev: 5' GAATATGGACCTTTGCAGTAC	TCAGTCTTGAGTTTCTTTCACAAAATCTACCTCCCACAATTCCGCTGGATATGCTAATCTGAGTTCAGAGGAATAACAAGTACTGCAAAGGTCCATATTC
	--qChip_FoxO3_8_Fow: 5' AGAACATCCTCACAGTCTAAG	--qChip_ FoxO3_8_Rev: 5'GCTGACTGTTAAGATGGG	AGAACATCCTCACAGTCTAAGACATTCTCTTCCTCTCCCCCTCCACTTCCCCCCCTCCTTTCCTCCTCTTCCCCACCCCCACCCCCCATCTTAACAGTCAGC
	--qChip_FoxO3_9_Fow: 5' CTCTCCAGGGTGCAGATG	--qChip_ FoxO3_9_Rev: 5' TCAACAACCTAGACACATAATC	CTCTCCAGGGTGCAGATGCCCTCTAGCTCTGAAAACTTTTCCGAGAAAGAACCAGGGTGAATCTTGGGCTCTGGACTGGATTATGTGTCTAGGTTGTTGA
	--qChip_FoxO3_10_Fow: 5' ACTTGGCTGAGGCAGGG	--qChip_ FoxO3_10_Rev: 5' AGGCTTGAACCCAGCCATCC	ACTTGGCTGAGGCAGGGGTTGGAGAACAGGTGTTGATGAACAGTGAATAACTTTTAAATATCCCCTGAACGTGAGAGTCAGGATGGCTGGGTTCAAGCCT
	--qChip_FoxO3_11_Fow: 5' TCGCTGTTACATCCTAGGG	--qChip_ FoxO3_11_Rev: 5' GAAAGCTGACAGAAGCTCTCTC	TCGCTGTTACATCCTAGGGAGAGCTGCCCTTGACACCTACGAGGTCCCCACACACAGACAGGCTGGGGTGAGGAGGATGAGAGAGCTTCTGTCAGCTTTC
	--qChip_FoxO3_12_Fow: 5' CATCGTTTCATGTCATATAAGG	--qChip_ FoxO3_12_Rev: 5' CATACAATACCTATTTATGTG	CATCGTTTCATGTCATATAAGGATTTGCTCACATAGGTATGCTCTGTATGTTTGGTCCCGTGTCATATAAGGGTGTATTCACATAAATAGGTATTGTATG

around Tal1 Binding

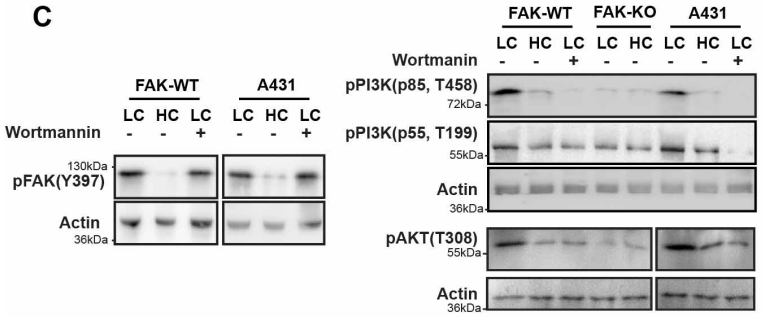

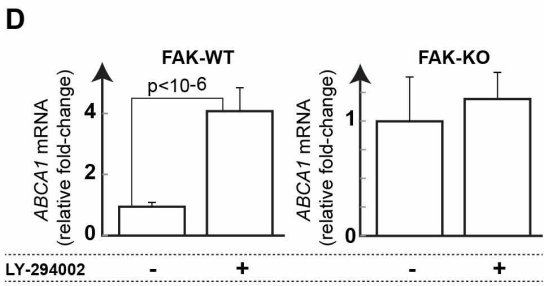

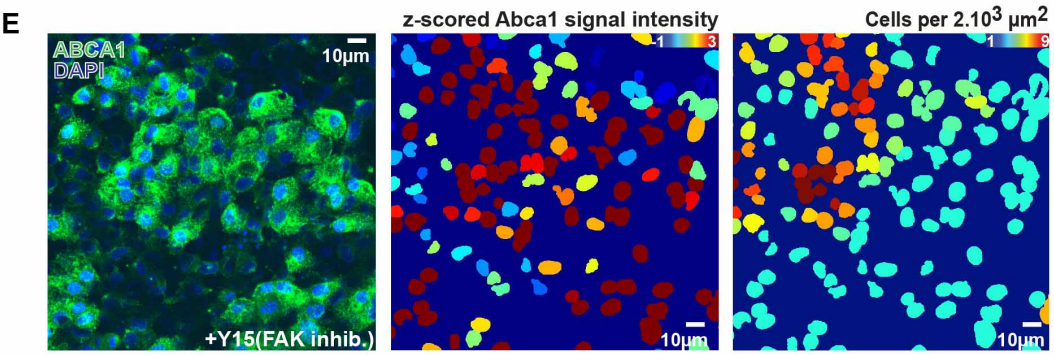

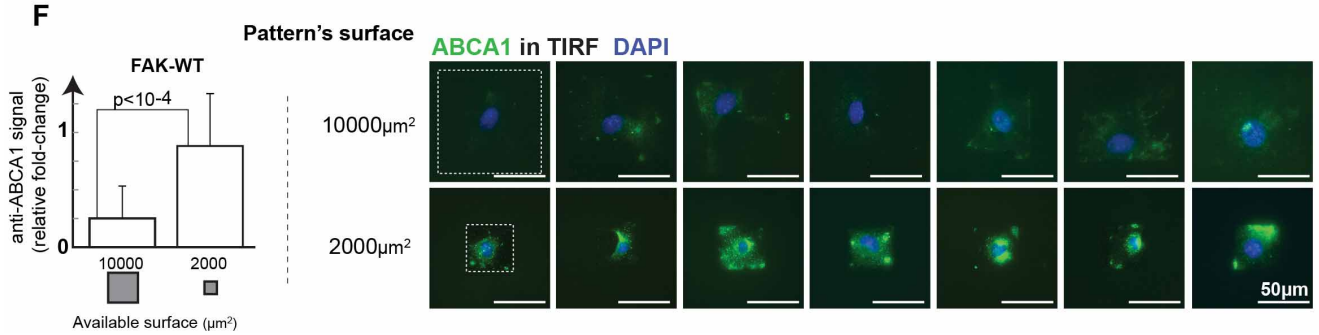

Extended Data Figure 2 | FAK suppresses ABCA1 expression in cells at low crowding via TAL1 and FOXO3 in a cell-intrinsic way. Related to Fig. 2. **a**, Percentage reduction of *Abca1* mRNA in FAK-KO cells upon silencing of 19 potential transcription factors. **b**, Table of primers used for qRT–PCR amplification of *Abca1* DNA and corresponding genomic position. **c**, Western blots of pFAK, pPI(3)K and pAKT levels in FAK-WT and FAK-KO MEFs, and A431 cells at low crowding, high crowding or low crowding + wortmannin. **d**, Real-time PCR quantification of *Abca1* mRNA shows that treatment with LY-294002 alleviates the inhibitory effect of FAK on *Abca1* transcription in cells (at low crowding) expressing FAK (s.d., $n = 4$ biological replicates each made of 3 technical replicates, $P < 10^{-6}$, *t*-test), whereas this treatment has no significant effect on *Abca1* transcription in cells that lack FAK (s.d., $n = 4$ biological replicates each made of 3 technical replicates, $P > 0.1$, *t*-test). **e**, Immunofluorescence imaging of ABCA1 over a population of A431 cells in the presence of Y15 FAK inhibitor and related projection of single cell measurements onto nuclear segmentations. **f**, Quantifications of Abca1 protein expression in FAK-WT cells adhering to micropatterned surfaces of large (10,000 μm^2) or small (2,000 μm^2) area (http://www.cytoo.com) at long distance from potentially secreting neighbouring cells. This shows that space constraints are sufficient to trigger differences in Abca1 expression (s.d., $n = 100$ cells, $P < 10^{-4}$, *t*-test).

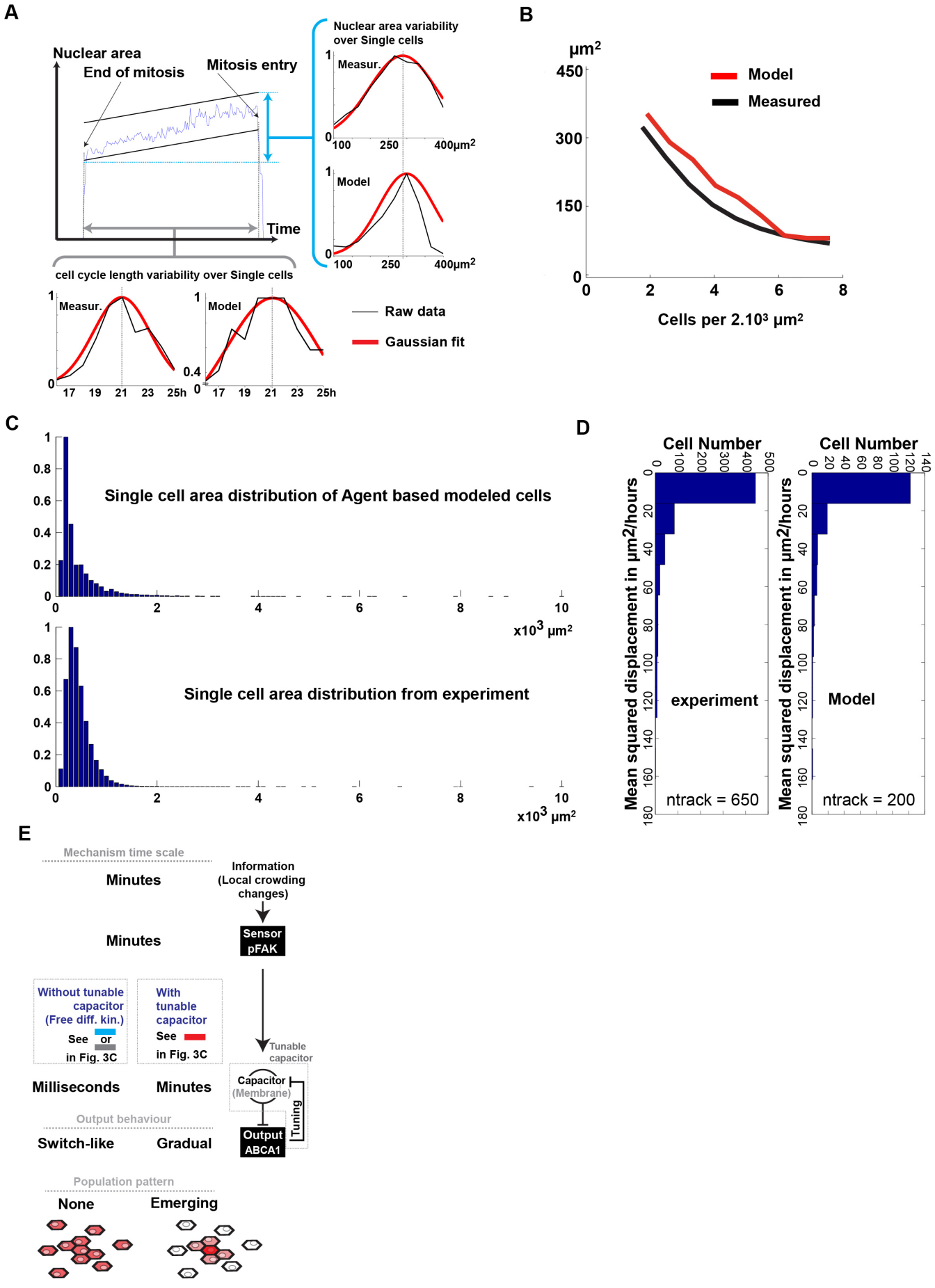

Extended Data Figure 3 | Agent-based modelled single cells show characteristics similar to tracked cells. **a**, Typical curve of the growth of the nucleus size of a single cell between two mitotic events (centre). Distribution of measured (number of tracks: 650) and agent-based modelled (number of tracks: 200) single-cell nucleus sizes (right histograms) and cell-cycle lengths (bottom histograms). Black, raw data, red, fitted Gaussian curve. Agent-based modelled cells and measured cells show similar distributions in cell-cycle length and nucleus size. **b**, Curve showing single-cell mean nuclear area against local cell crowding of measured (black, number of cells: $>10^4$) and agent-based modelled cells (red, number of cells: $>10^3$). **c**, Histograms of single-cell area distribution of measured (number of cells: $>10^4$) and agent-based modelled cells (number of cells: $>10^3$) showing that distribution of emerging cell areas of modelled cells are matching those of measured cells even for extreme values. **d**, Histograms of single-cell mean square displacement distribution of measured (number of tracks: 650) and agent-based modelled cells (number of tracks: 200). **e**, Timescales of information sensing and processing steps in the FAK–ABCA1 system. Absence of a capacitor does not allow gradual patterns to emerge (switch-like behaviour).

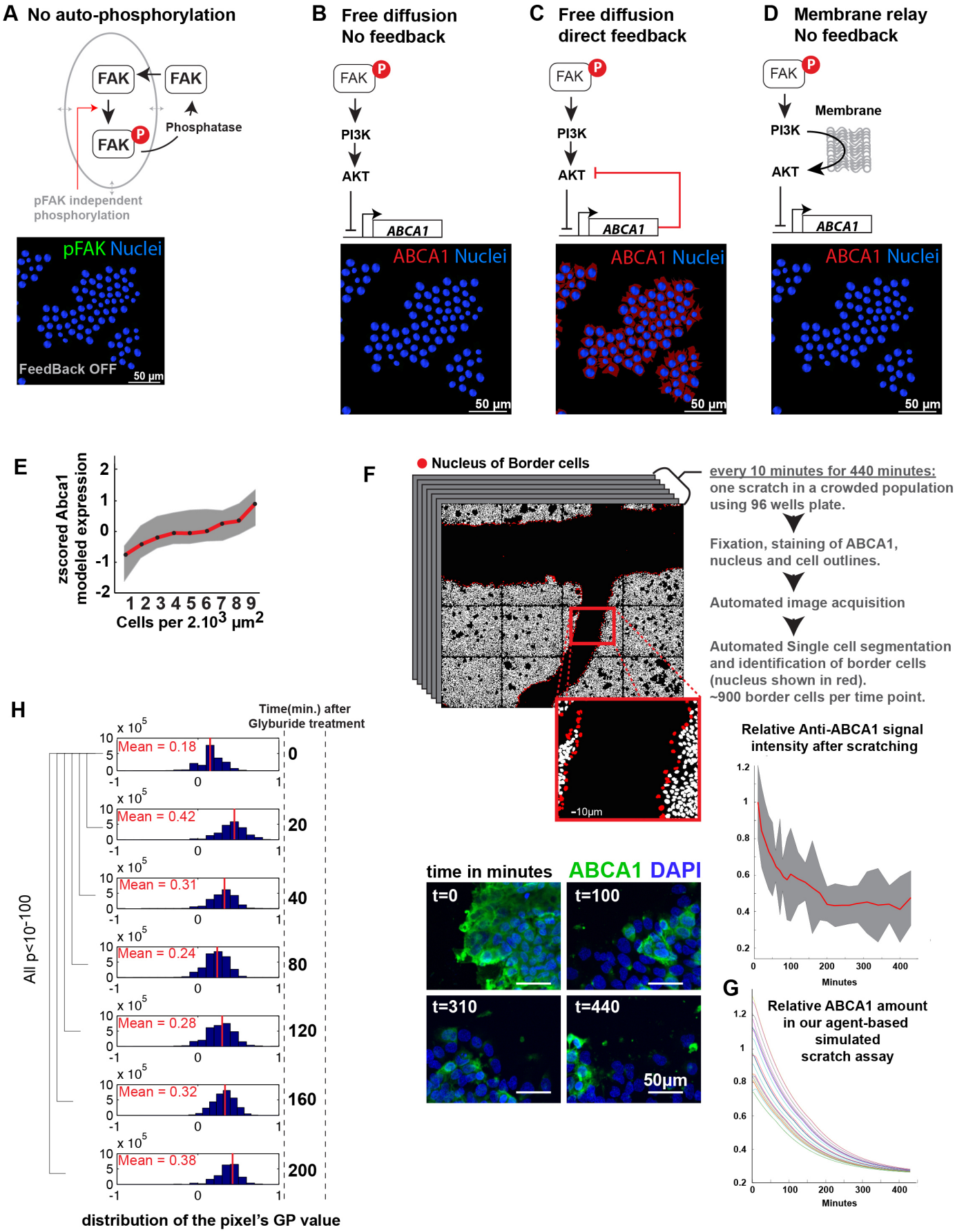

Extended Data Figure 4 | Alternative models do not lead to the emergence of gradual patterns in ABCA1 expression, and the full model recapitulates experimentally observed dynamics of reduction in ABCA1 expression in scratch assays. Conclusions are parameter-independent, for details see mathematical appendix in the Supplementary Information. **a**, A FAK activation model without autophosphorylation does not result in a pFAK pattern in an agent-based modelled cell population. **b**, A FAK–ABCA1 model based on free diffusion of signalling molecules without or with **c**, addition of a putative direct inhibitory effect of ABCA1 on its own suppression does not result in a patterning of ABCA1 expression. **d**, Introduction of a membrane relay for AKT activation without ABCA1 feedback on the membrane relay does not result in a patterning of ABCA1 expression. **e**, Simulated single-cell ABCA1 variability over local crowding is similar to the variability seen in our experiments (see Fig. 2d). **f**, Scratch assays, at which cells at high crowding suddenly become exposed to free space to spread and followed over time, show that reduction of ABCA1 levels in these cells has a half-maximum effect at ~50 min, and full effect at ~200 min. **g**, This is in agreement with simulations of scratch assays using our cell-intrinsic Agent-based model of the FAK–ABCA1 system. The process was iterated thousands of times with random starting levels of ABCA1 similar to the variability seen in the experimental scratch assay. 20 representative curves are shown. In the simulations, it takes ~150 min for the disappearance of half of ABCA1. **h**, Distributions of pixel GP values of FAK-KO cells stained with Laurdan at different time-points after treatment with glyburide. After just 20 min of drug treatment, the membranes of these cells become more ordered ($P < 10^{-100}$, *t*-test, pixel distributions at each time point are made from 2×10^3 cells).

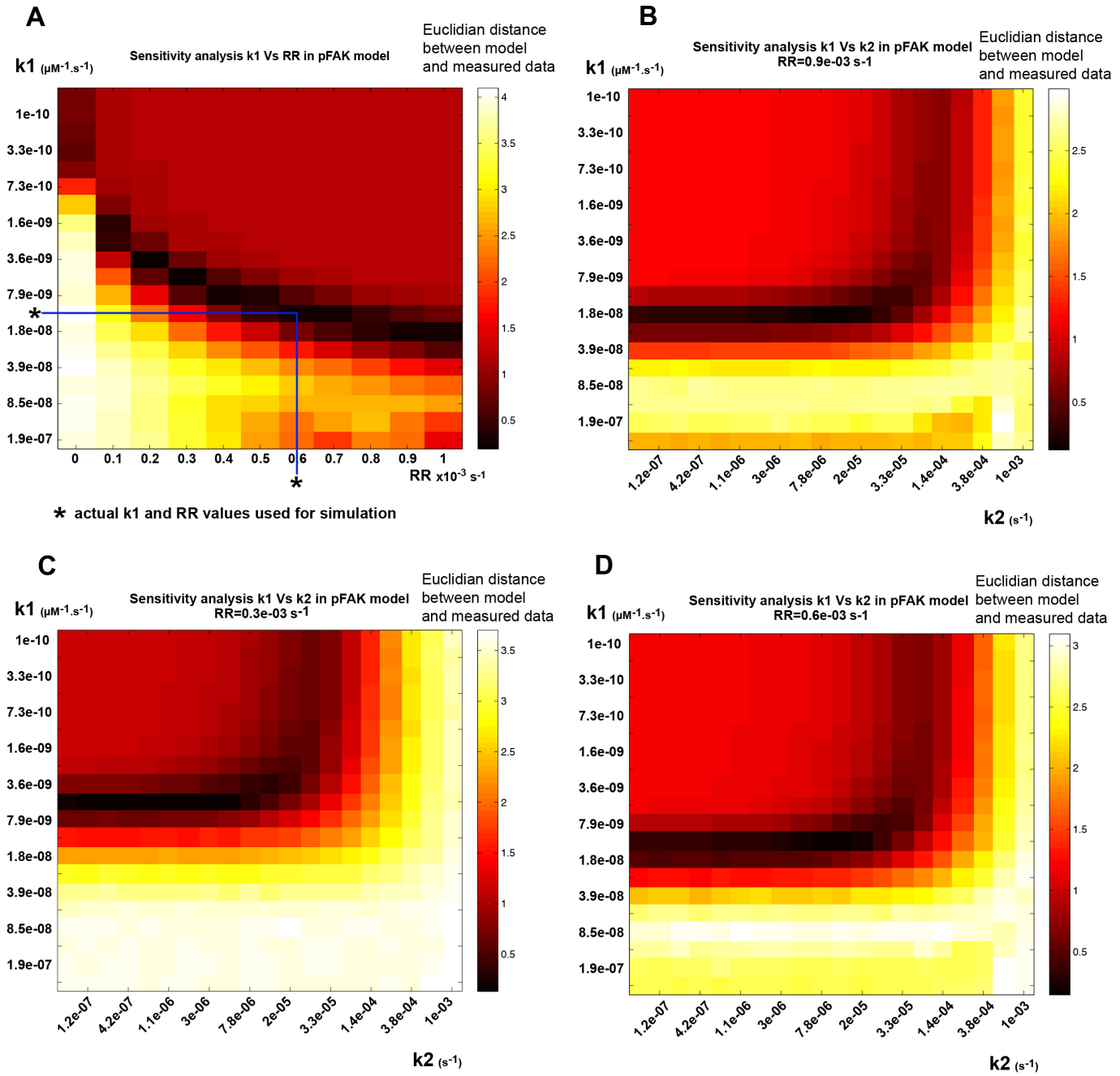

Extended Data Figure 5 | Sensitivity analysis of the FAK activation model. **a**, Heat map representing Euclidian distance between modelled and measured levels of pFAK in single cells as a function of local crowding when autophosphorylation constant k_1 and removal rate RR varies. Stars represent the values used for further modelling; any pair of k_1-RR values with the same low Euclidian distance will lead to the proper pFAK pattern. **b**–**d**, Same analysis for k_1 and the FAK-independent phosphorylation of FAK rate k_2 for a fixed RR value shows that FAK-independent phosphorylation of FAK has no effect on the formation of a pFAK pattern even if k_2 is bigger than k_1 by several orders of magnitude.

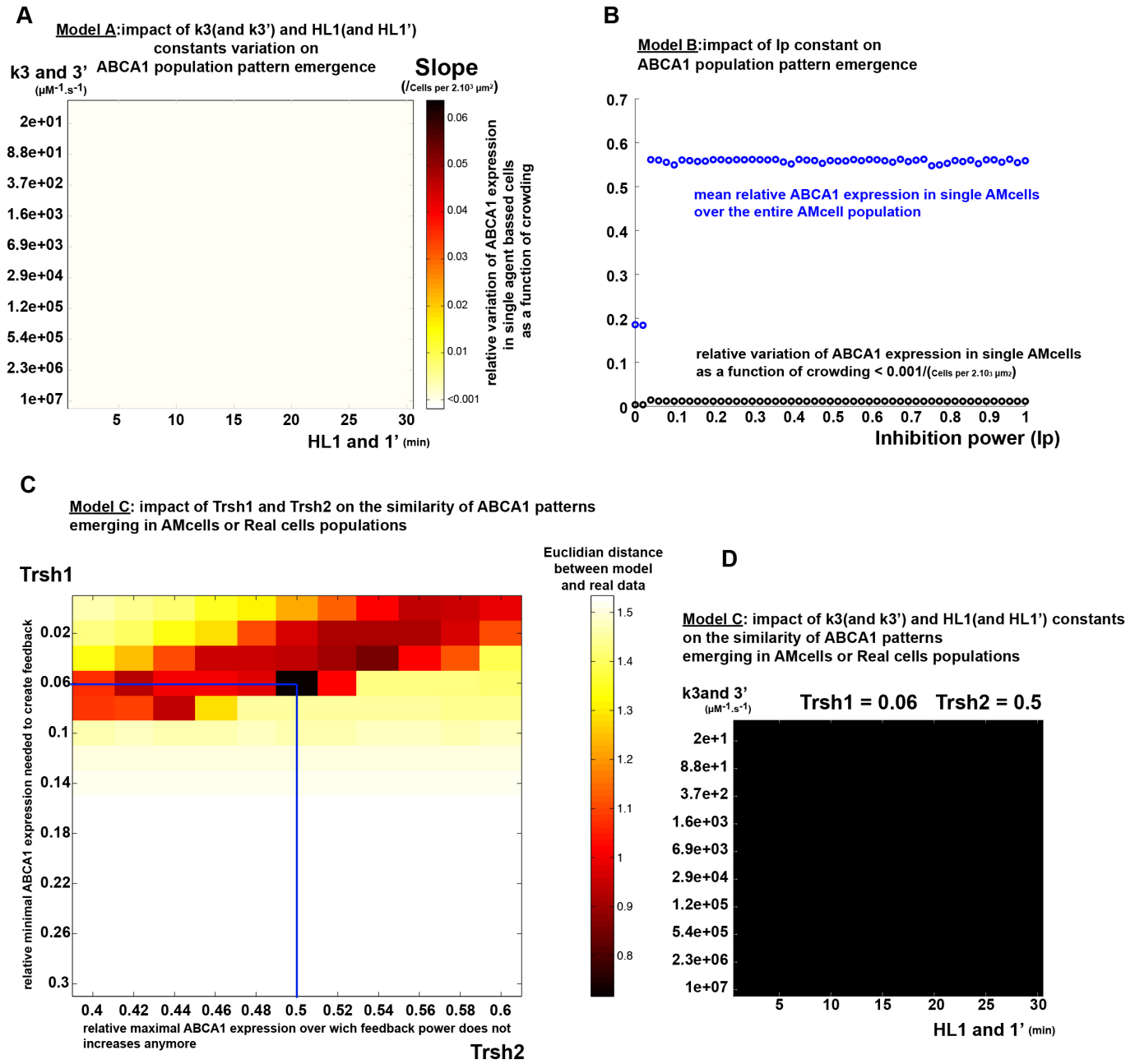

Extended Data Figure 6 | Sensitivity analysis of the FAK to ABCA1 expression models. **a**, Heat map representing the slope of ABCA1 expression against local cell crowding when k_3 and 3′ and HL1 and 1′ vary over an extreme range of values for model A. This demonstrates that such topology cannot lead to emergence of gradual expression patterns ABCA1 expression as a function of local cell crowding. **b**, Mean relative ABCA1 expression in agent-based modelled cells as a function of its inhibition power (Ip) in model B, where ABCA1 would be able to directly inhibit activation of AKT (or PI(3)K). This demonstrates that such direct feedback only leads to switch-like behaviour where ABCA1 is either expressed or not in all cells of the population, independent of local cell crowding. Inhibition power represents the ABCA1 competitive inhibitory power. **c**, Heat map representing Euclidian distance between modelled and measured levels of ABCA1 in single cells as a function of local crowding when Trsh1 and Trsh2 vary in model C. **d**, The capacity of model C to generate a gradual expression pattern (low Euclidian distance is black) does not depend on k_3 and 3′, and HL1 and 1′, demonstrating the central role of the membrane relay for gradual patterns to emerge.

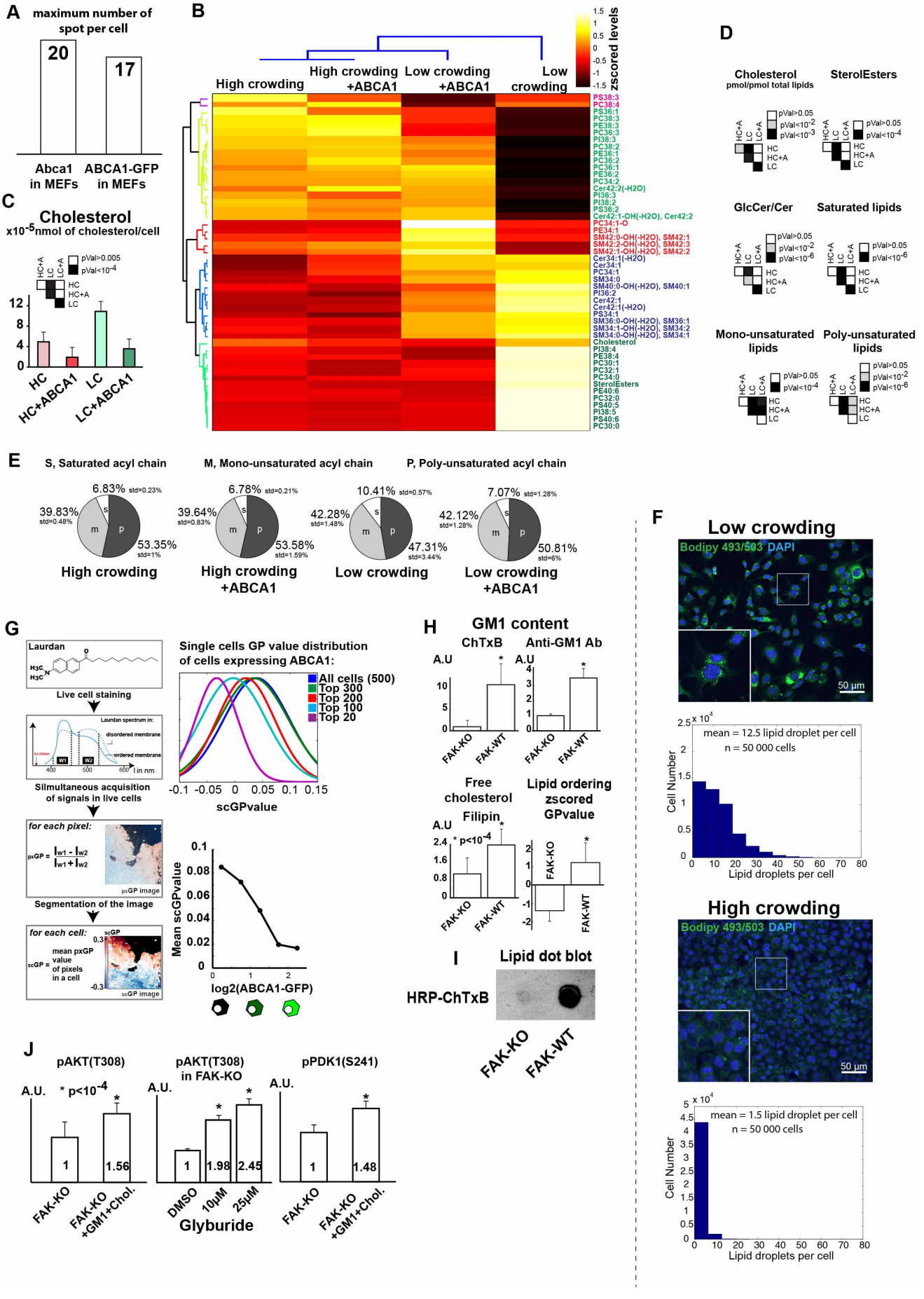

Extended Data Figure 7 | The FAK–ABCA1 system adapts membrane lipid composition, ordering and signalling to local crowding. Related to Fig. 4. **a**, Histogram of transcript copy number (number of spots) per cell determined with bDNA single-molecule FISH against endogenous *Abca1* in cells at high crowding, or against *ABCA1–GFP* transcripts in cells at low crowding transfected with the pEGFP-N1-ABCA1 construct. This shows that plasmid-driven *ABCA1–GFP* expression in cells at low crowding does not exceed that of endogenous *Abca1* levels in cells at high crowding. **b**, Hierarchical clustering of lipid profiles of mouse embryonic fibroblasts grown at high crowding or low crowding conditions and transiently expressing ABCA1 from a plasmid (+ABCA1) or not. The clustergram shows the 48 lipid species that represent 80% of the total lipid amount. Colours correspond to pmol/pmol total lipid *z*-scored over the four conditions, colours of lipid names refer to their clusters. For complete lipid mass spectrometry data, see Supplementary Table 3. **c**, Histograms displaying the quantity of free cholesterol in nmol per cell ($n = 4$ biological replicates, each the mean of 4 technical replicates, s.d.). **d**, *P* values related to the bar graphs in Fig. 4c. **e**, Pie charts representing the percentage of saturated, monounsaturated and polyunsaturated lipids for the four different conditions. **f**, Fluorescence imaging using Bodipy 493/503 dye of lipid droplets in low crowding ($n = 5 \times 10^4$ single cells) or high crowding conditions ($n = 5 \times 10^4$ single cells). This confirms that cells at low crowding contain a larger amount of cholesteryl-esters, which are stored in lipid droplets. **g**, Diagram summarizing the method to measure membrane ordering of a formaldehyde fixed population of cells at the single-cell level (left flow chart). Distributions of single-cell GP values for groups of cells that are the top 20, 100, 200, 300 ABCA1–GFP expressing cells compared to all cells (top right distributions, $n = 500$ cells) and curve showing the relationship between single-cell ABCA1 expression and scGP value (bottom right curve, $n = 500$ cells). **h**, Image-based quantification of free cholesterol (filipin), GM1 content (cholera toxin B binding or anti-GM1 antibody) and lipid ordering (Laurdan, as in panel **d**) in single MEFs with (FAK-WT) or without FAK (FAK-KO). $n = 4$ experiments, each $>10^4$ cells. **P* values (*t*-test) $< 10^{-4}$. **i**, Because some GM1 may not be accessible in formaldehyde-fixed cells, we performed dot blot analysis of lipid extracts from FAK-KO and FAK-WT cells using HRP-conjugated cholera toxin B. This indicates that FAK-WT cells have higher levels of GM1 than FAK-KO cells. **j**, pAKT and pPDK1 immunostaining in cells without FAK (FAK-KO) exogenously loaded with GM1 and cholesterol (FAK-KO + GM1 + Chol.), treated with DMSO, or with 10 and 25 μM glyburide in DMSO ($n = 3$ experiments, each 10^4 cells, s.d., **P* values (*t*-test) $<10^{-4}$.

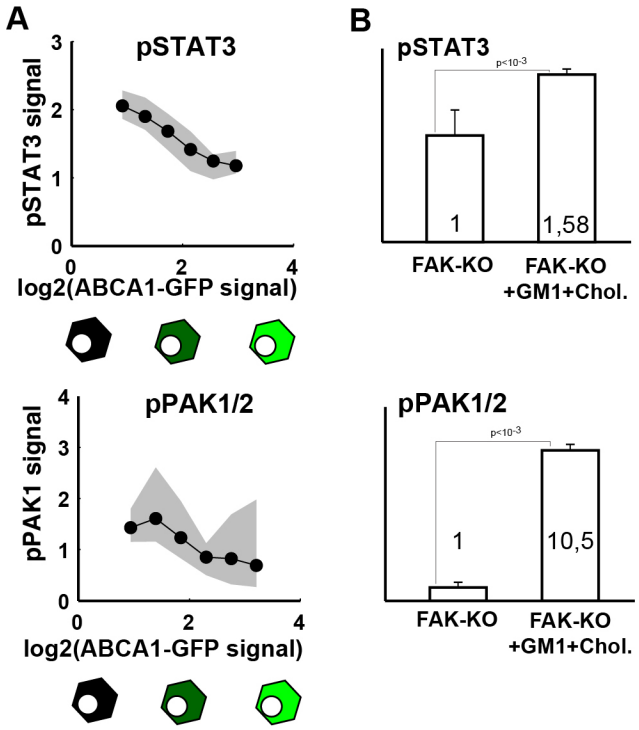

Extended Data Figure 8 | Phosphorylation of STAT3 and PAK1/2 are sensitive to ABCA1-mediated membrane perturbation. **a**, Curve showing the relationship between ABCA1–GFP expression and phosphorylated STAT3 (T705) and PAK1/2 (T423/T402) amounts in single cells. **b**, Quantification of immunostaining of phosphorylated STAT3 (T705) and PAK1/2 (T423/T402) amounts in FAK-KO cells after exogenous loading of the plasma membrane with cholesterol and GM1 (s.d., $n = 4$ experiments, each with 10^4 cells, *t*-test).

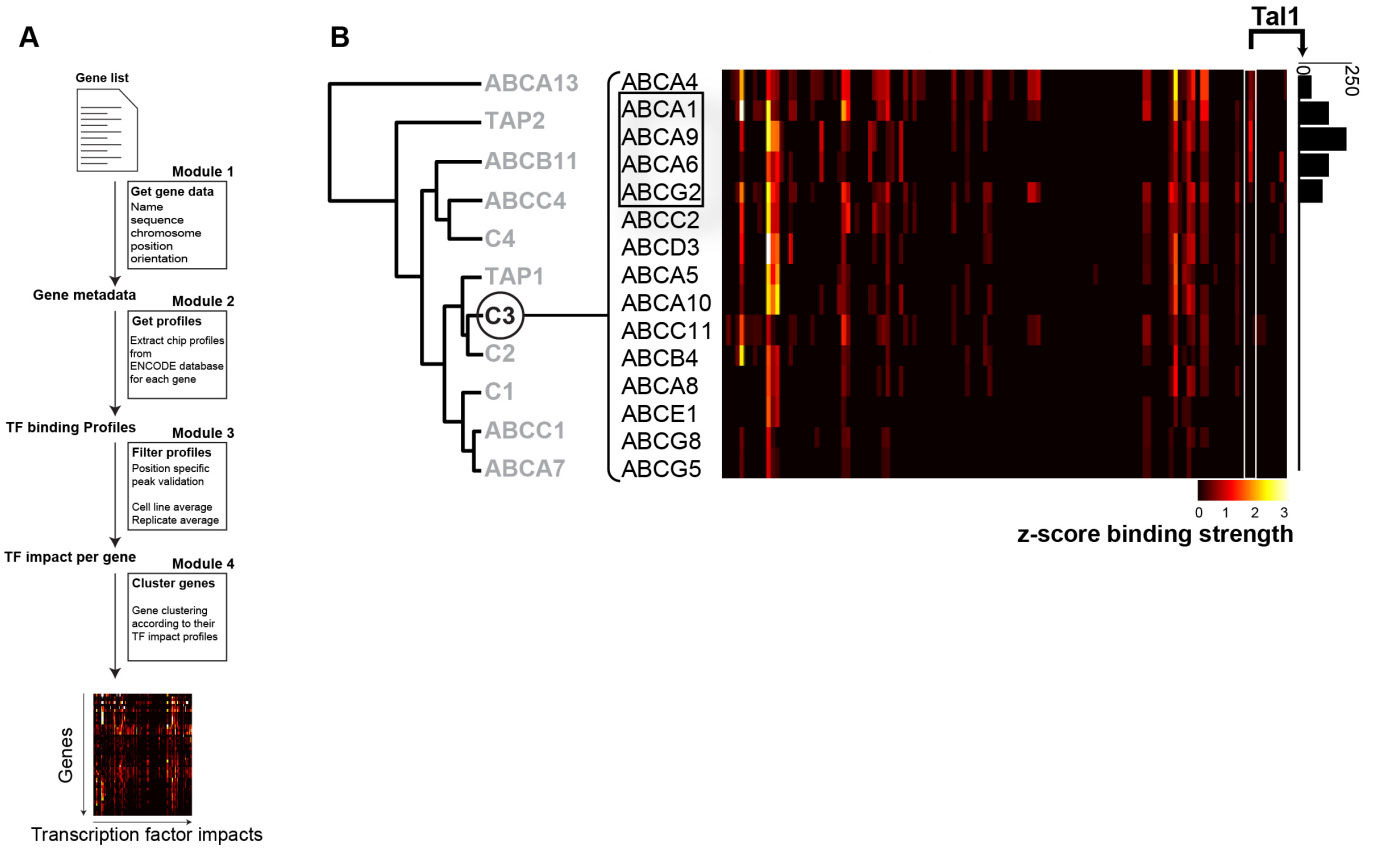

Extended Data Figure 9 | Hierarchical clustering of human ABC transporters according to 118 transcription factor binding profiles from the ENCODE database. **a**, Diagram of the algorithm used to generate ABC transporter clusters. **b**, Heat map of the cluster of ABC transporters containing ABCA1, A9, A6 and G1 that share Tal1 binding (see bar graph representation of Tal1 binding on the right). These 4 ABC transporters are the same 4 ABC transporters that were found higher expressed in cells lacking FAK (FAK-KO) (see Extended Data Fig. 1c).